

AD-762 019

A METHOD OF SOLUTION FOR HYDRODY-
NAMICS AND RADIATION DIFFUSION AS A
MULTI-MATERIAL PROBLEM IN ONE
DIMENSION

Scott Thomas Bennion

Utah University

Prepared for:

Advanced Research Projects Agency
Atomic Energy Commission
Rome Air Development Center

June 1971

DISTRIBUTED BY:

NTIS

National Technical Information Service
U. S. DEPARTMENT OF COMMERCE
5285 Port Royal Road, Springfield Va. 22151

**BEST
AVAILABLE COPY**

AD 762019

A METHOD OF SOLUTION
FOR
HYDRODYNAMICS AND RADIATION DIFFUSION
AS A MULTI-MATERIAL PROBLEM IN ONE DIMENSION

by

Scott Thomas Bennion

Reproduced by
**NATIONAL TECHNICAL
INFORMATION SERVICE**
U S Department of Commerce
Springfield VA 22151

June 1971

UTEC-CSc-71-114

This research was supported in part by the University of Utah Computer Science Division and by the Advanced Research Projects Agency of the Department of Defense, monitored by Rome Air Development Center, Griffiss Air Force Base, New York, 13440, under contract F30602-70-C-0300, ARPA Order Number 829.

AD 762019

A METHOD OF SOLUTION
FOR
HYDRODYNAMICS AND RADIATION DIFFUSION
AS A MULTI-MATERIAL PROBLEM IN ONE DIMENSION

by

Scott Thomas Bennion

Reproduced by
**NATIONAL TECHNICAL
INFORMATION SERVICE**
U S Department of Commerce
Springfield VA 22151

June 1971

UTEC-CSc-71-114

This research was supported in part by the University of Utah Computer Science Division and by the Advanced Research Projects Agency of the Department of Defense, monitored by Rome Air Development Center, Griffiss Air Force Base, New York, 13440, under contract F30602-70-C-0300, ARPA Order Number 829.

This report reproduces a thesis of the same title submitted to the Department of Electrical Engineering, Division of Computer Science, University of Utah, in partial fulfillment of the requirements for the degree of Doctor of Philosophy.

ACKNOWLEDGMENTS

In addition to the support given this project by the University of Utah and the Advanced Research Projects Agency, part of this work was also sponsored by Los Alamos Scientific Laboratory, Los Alamos, New Mexico, under AEC Contract W-7405-ENG-36.

Thanks is given to all those at Los Alamos, University of Utah, and Montana State who have helped and assisted me with this project.

TABLE OF CONTENTS

ACKNOWLEDGMENTS	iii
ABSTRACT	vi
Chapter 1: INTRODUCTION	1
1.1 Nomenclature	4
1.2 Units of Measure	5
1.3 Physical Constants	5
1.4 Conversion Factors	5
Chapter 2: SYSTEM OF SOLUTION FOR HYDRODYNAMICS AND RADIATION DIFFUSION	6
2.1 Partial Differential Equations	7
2.2 Hydrodynamic Difference Equations	8
2.3 Radiation Diffusion Difference Equations	11
2.4 Implicit Solution for Radiation Diffusion	18
2.5 Time Advancement Procedure	20
Chapter 3: AREA, VOLUME AND CENTER OF MASS CALCULATIONS	25
3.1 Plane Geometry	25
3.2 Cylindrical and Spherical Geometry	29
3.3 Change in Volume at the Boundaries	30
Chapter 4: TIME STEP SIZE DETERMINATION	31
4.1 Courant-Friedricks-Levy Hydrodynamic Stability Criterion.	31
4.2 Hydrodynamic Zone Increment Change Restriction	32
4.3 Temperature Change Restriction	34
4.4 Doubling Restriction	35
4.5 Print Restriction	36

4.6	Maximum Restriction	37
4.7	Hold Time Restriction	38
4.8	Time Step Size Selection	38
Chapter 5: MATERIAL PROPERTIES		39
5.1	Equation of State	39
5.2	Mean Free Path	44
5.3	Opacity	49
Chapter 6: SOURCE TERM		51
6.1	Energy-Time Profile	51
6.2	Temperature-Time Profile	53
Chapter 7: COMPUTER CALCULATIONS		55
7.1	Radiation Diffusion Calculations	55
7.2	Hydrodynamic Calculations	74
7.3	Combined Radiation Diffusion and Hydrodynamics	89
7.4	Summary	96
Chapter 8: CONCLUSION AND AREAS FOR FUTURE RESEARCH		102
BIBLIOGRAPHY		109

ABSTRACT

with various for future work
This dissertation formulates and reports upon the implementation of a numerical system for the solution of hydrodynamics and radiation diffusion as a multi-material problem in one dimension. A parametric system is developed in which the program parameters may be dynamically altered and studied as to their worth and effectiveness. The system is designed specifically for use within an interactive man-machine environment wherein the user becomes an integral part of the final solution.

1.

INTRODUCTION

The largest and fastest computers have always been used for the solution of partial differential equations, especially non-linear equations which are used to describe some physical phenomenon in time and space. Computer programs for this class of problems are large, and their creation requires a joint effort of many individuals over long periods of time, most of which is consumed by the debugging process. Once such a program has been developed, its use requires a great deal of data to specify the desired physical system. It also requires an intimate knowledge of the workings of the program and a vast amount of intuition and experience into the mechanics of the physical processes involved. Even without difficulties, such problems run for hours at a time on the most modern computers in the typical batch mode. At some time after what may develop into days and weeks of aborts, restarts, parameter changes, program patches, reconfigurations and the like, the user finally acquires several edge feet of printed output and perhaps a few computer generated graphs which represent the solution to his problem. He must then examine, plot and otherwise become familiar with this output data and make judgments as to its validity and applicability within the constraints of the system being designed or simulated.

With the advent of multiprogramming, time-sharing and real-time problem solving at a remote console, new hardware and software tools are being developed to allow the programmer and the user to become an active part of the checkout and running process of a program. While this document reports on the development of a medium size program within the rudiments of such an interactive environment, its primary emphasis is placed upon the derivation of a numerical system for the solution of hydrodynamics and radiation diffusion as a multi-material problem in one dimension. The system is developed parametrically in a very general form. Thus, the user is able to dynamically configure the system into a form best suited for his immediate needs through the program parameters. The technique is not unlike that of adjusting and tuning a fine piece of complex mechanical equipment. It also inherits many of the disadvantages of such mechanical systems, primarily the difficulty of dynamically changing the program. More will be said on this and the requirements for man-machine systems for these types of computations in the concluding chapter.

The development of this system has taken place over the period of some three years. During this time, a number of preliminary computer programs and interactive graphical display systems have been written and developed. The work on this system originated at Los Alamos Scientific Laboratories in New Mexico. It then moved to the University of Utah and subsequently to Montana State University. Computer programs of the system are currently operational at Los Alamos and at Montana State University through remote graphics facilities in connection with the University of Utah.

Over this period of development, many ideas and techniques have been explored, tested, accepted and rejected. This is particularly true with respect to the physics and the subsequent numerical treatment of interface conditions. As program parameters were tested and as comparative analyses were made with other systems and solutions, both analytical and empirical, different techniques and features were incorporated. These changes are the results of several years of experience and formal education not only in the areas of physics, mathematics and analysis, but also in computer science.

In chapter 2, the difference approximations to the partial differential equations are derived and the complete system of solution is presented. The remaining chapters are used to give the details of the auxiliary calculations. The volume and mass center calculations are given in chapter 3, and chapter 4 discusses the time step selection procedure and the associated restrictions and control parameters. Chapter 5 deals with the material properties and the calculational aspects of the various thermodynamic and opacity coefficients. Chapter 6 discusses the various ways of specifying and calculating the source terms, and chapter 7 is a summary of calculational results. Chapter 8 concludes with some comments on future research areas, particularly with respect to the man-machine systems alluded to above.

This chapter is concluded with definitions of the symbols and units of measure used throughout the remainder of the text.

1.1 Nomenclature

Symbol	Description	Unit of Measure
A	area	cm^2
b'	gas constant	j/Kv-gm
e	internal energy per unit mass	j/gm
E	internal energy	j
m	mass	gm
p	pressure	j/cc
r	radius	cm
s	source per unit mass	j/gm
S	source	j
t	time	sh
u	velocity	cm/sec
v	specific volume	cc/gm
V	volume	cc
x	space	cm
\dot{x}	velocity	cm/sh
\ddot{x}	acceleration	cm/sh^2
ρ	density	gm/cc
θ	temperature	Kv
ϕ	fourth power of temperature	Kv^4
κ	opacity	cm^2/gm
$\frac{1}{\lambda}$	Rosseland mean of the mean free path	cm

1.2 Units of Measure

gm	gram
cm	centimeter
j	jerk
Kv	kilovolt
sh	shake

1.3 Physical Constants

a	radiation density constant	.013732 j/cm-Kv ⁴
c	velocity of light	299.7925 cm/sh

1.4 Conversion Factors

$$1 \text{ atmosphere} = 10^{-10} \text{ j/cm}^3 = 10^{-3} \text{ kilobars}$$

$$1 \text{ j} = 10^{16} \text{ ergs}$$

$$1 \text{ Kv temperature equivalent} = 1.16049 \times 10^7 \text{ }^\circ\text{K}$$

$$1 \text{ sh} = 10^{-8} \text{ seconds}$$

2.

SYSTEM OF SOLUTION

FOR

HYDRODYNAMICS AND RADIATION DIFFUSION

A set of difference equations and a system for their solution is developed for hydrodynamics and radiation diffusion. The momentum equation is differenced in a natural way assuming an average density at the interface in lieu of the standard area over mass technique. Thus, an actual pressure gradient is computed between pressure points calculated at centers of mass.

From the beginning, the goal was to difference the energy equation in terms of the temperature to the fourth power. This approach was selected because it appeared to be the most natural and least complicated in contrast with the more traditional differencing schemes in terms of the temperature or change in temperature. A fully parameterized system was developed in very general terms. This permits detailed studies into the effects of time differences, interpolation and extrapolation functions, smoothing functions and the like. In addition, an iterative procedure is employed to preserve the nonlinearities with respect to the energy derivatives, pressure and mean free path.

The complete set of difference equations together with boundary conditions are solved in a well defined sequence over an incremental unit of time. The solution is represented by temperatures, pressures and densities as functions in time and space.

2.1 Partial Differential Equations

The mass, momentum, and energy conservation equations are solved together in a Lagrangian system where the motion of fixed mass points is followed in plane geometry. The substantial derivative forms of these equations in vector notation [1] are:

$$\frac{d\rho}{dt} = -\rho (\nabla \cdot \vec{u}) \quad (2.1)$$

$$\rho \frac{d\vec{u}}{dt} = -\nabla p, \quad (2.2)$$

$$\rho \frac{d\varepsilon}{dt} = -p(\nabla \cdot \vec{u}) - \nabla \cdot \vec{q} + \rho \frac{ds}{dt}, \quad (2.3)$$

where the viscous pressure and gravitational terms have not been included. The Rosseland radiation diffusion equation [2],

$$\vec{q} = -\frac{ac}{3} \bar{\lambda} \nabla \phi \quad (2.4)$$

is used for the flux term and the standard conduction term is omitted.

Equations (2.1) and (2.3) are combined to give a system of equations for hydrodynamics and radiation diffusion.

$$\rho \frac{d\vec{u}}{dt} = -\nabla p, \quad (2.5)$$

$$\rho \frac{d\varepsilon}{dt} = -\rho p \frac{dv}{dt} + \nabla \cdot \frac{ac}{3} \bar{\lambda} \nabla \phi + \rho \frac{ds}{dt}. \quad (2.6)$$

2.2 Hydrodynamic Difference Equations

Equation (2.5) is differenced to describe the motion of interfaces defining the constant mass zones. Figure 1 illustrates the differencing scheme where the center of mass of a zone, denoted by the half index $i+\frac{1}{2}$, gives the position of the temperature, pressure and density. The interfaces delineate the mass zones and are referenced through the integral indices i and $i+1$. Note that these interfaces are fictitious interfaces arbitrarily constructed to obtain difference equations representative of the actual differential equation given by equation (2.5). Real interfaces between material types are maintained and included within the difference scheme.

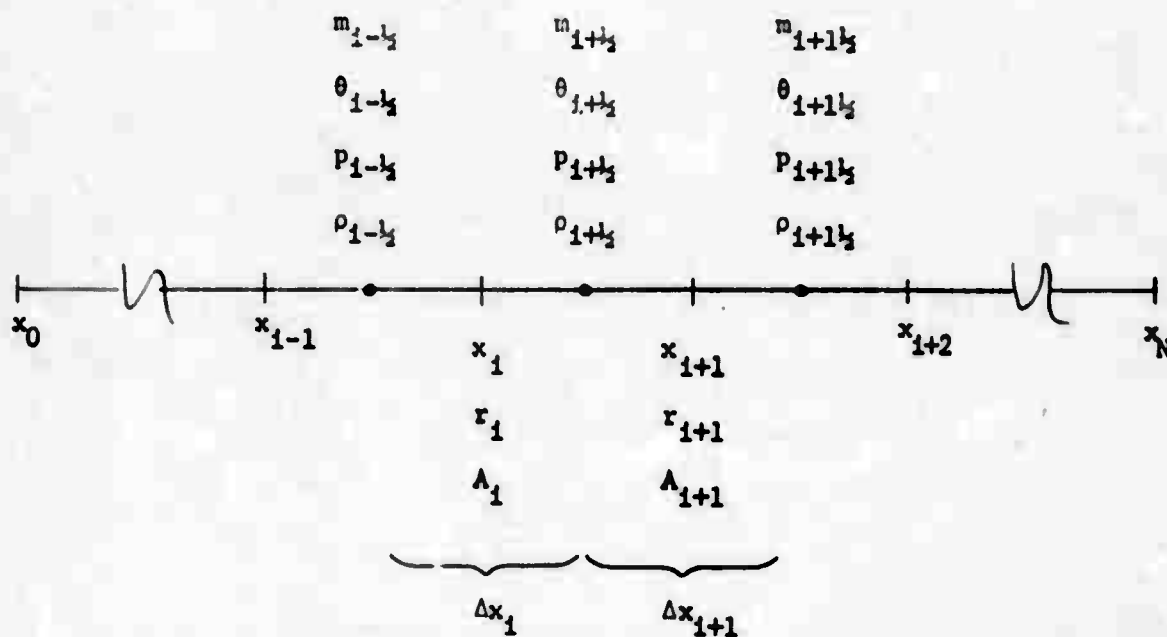


Figure 1

The acceleration, velocity, and spatial coordinates are calculated explicitly at each interface through the following sequence of equations:

$$\ddot{x}_1^n = \frac{V_{i+1/2}^n + V_{i-1/2}^n}{m_{i+1/2} + m_{i-1/2}} \frac{p_{i-1/2}^n - p_{i+1/2}^n}{\Delta x_1^n} \quad (2.7)$$

$$\dot{x}_1^{n+1/2} = \dot{x}_1^{n-1/2} + \ddot{x}_1^n \frac{\Delta t^{n+1/2} + \Delta t^{n-1/2}}{2}, \quad (2.8)$$

$$x_1^{n+1} = x_1^n + \dot{x}_1^{n+1/2} \Delta t^{n+1/2}, \quad (2.9)$$

where the superscript n denotes the time $t = t^n$ with

$$t^{n+1} = t^n + \Delta t^{n+1/2}. \quad (2.10)$$

Equation (2.7) is the one-dimensional difference form of equation (2.5) which describes the motion of the interface at x_1 between the adjacent mass zones whose centers of mass are at $x_{i-1/2}$ and $x_{i+1/2}$. Given the new space coordinates x_1^{n+1} and x_{i+1}^{n+1} , the new volume $V_{i+1/2}^{n+1}$ is calculated taking into account the dimensions of the zone $i+1/2$.

The program is capable of calculating the volume elements in one of three geometries: plane, cylindrical and spherical. In plane geometry, the radius of the container, often referred to as a pipe, may be constant or change in a linearly continuous or discontinuous fashion as shown in figure 2. This flexibility in cross section permits actual physical systems to be modeled more accurately with respect to volumes and areas, introducing a two-dimensional affect. Note however, that the program assumes that the user will proceed with caution and good physical intuition.

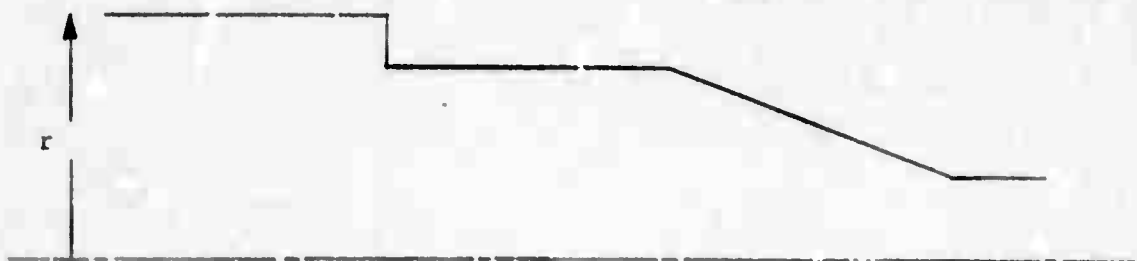


Figure 2

The details of these calculations will be presented later in chapter 3.

Given the new volume, an average density

$$\rho_{i+\frac{1}{2}}^{n+1} = \frac{m_{i+\frac{1}{2}}}{v_{i+\frac{1}{2}}^{n+1}} = \frac{1}{v_{i+\frac{1}{2}}^{n+1}} \quad (2.11)$$

and change in specific volume

$$\Delta v_{i+\frac{1}{2}}^{n+\frac{1}{2}} = \frac{v_{i+\frac{1}{2}}^{n+1} - v_{i+\frac{1}{2}}^n}{m_{i+\frac{1}{2}}} \quad (2.12)$$

are calculated for use within the diffusion equation.

The motion of the boundary interfaces is dependent upon boundary pressure conditions of the form

$$p = p(t), \quad (2.13)$$

where $p(t)$ is given by a user supplied subroutine. Thus, at spatial position $i = 0$,

$$x_0^n = v_{\frac{1}{2}}^n \frac{p(t^n)_0 - p_{\frac{1}{2}}^n}{(x_{\frac{1}{2}}^n - x_0^n)/\delta_0}, \quad (2.14)$$

and, likewise at $i = N$,

$$\ddot{x}_N^n = v_{N-1/2}^n \frac{p_{N-1/2}^n - p(\tau^n)_N}{(x_N^n - x_{N-1/2}^n)/\delta_N} \quad (2.15)$$

The velocities and space coordinates are calculated using equations (2.8) and (2.9). The change in volumes at the boundaries, $\Delta V_0^{n+1/2}$ and $\Delta V_N^{n+1/2}$ are then calculated over the respective intervals (x_0^n, x_0^{n+1}) and (x_N^n, x_N^{n+1}) in order to obtain the work done by the boundary pressures upon the adjacent zones. These energy terms

$$\Delta Sp_0^{n+1/2} = p(\tau^n)_0 \Delta V_0^{n+1/2}, \text{ and} \quad (2.16)$$

$$\Delta Sp_N^{n+1/2} = -p(\tau^n)_N \Delta V_N^{n+1/2} \quad (2.17)$$

are simply added to the source terms of the first and last zone, respectively.

2.3 Radiation Diffusion Difference Equations

The integration of equation (2.6) over a homogeneous volume element and the application of the divergence theorem yields

$$m \frac{dc}{dt} = -mp \frac{dv}{dt} + \frac{ac}{3} \int_A \frac{1}{\lambda} \nabla \phi \cdot \vec{n} dA + m \frac{dS}{dt} \quad (2.18)$$

In one dimension

$$\nabla \phi \cdot \vec{n} = \pm \frac{\partial \phi}{\partial x}; \quad (2.19)$$

therefore,

$$m \left\{ \frac{\partial c}{\partial t} \frac{dv}{dt} + \left[\frac{dc}{dv} + p \right] \frac{dv}{dt} \right\} = \pm \frac{ac}{3} \int_A \frac{1}{\lambda} \frac{\partial \phi}{\partial x} dA + \frac{dS}{dt}, \quad (2.20)$$

with the sign being determined by the direction of integration.

The time advancement scheme is parameterized so that the range from explicit through fully implicit differencing can be examined. This generalized differencing permits a detailed analysis of the numerical processes including stability questions [3]. Also, direct comparisons between the explicit, implicit and time-centered schemes can be made dynamically with the same program on the same physical problem.

The finite difference form of equation (2.20) for a typical interior zone is:

$$\begin{aligned}
 & \left\{ \left(\frac{\Delta \epsilon}{\Delta \phi} \right) \Delta \phi + \left(\frac{\Delta \epsilon}{\Delta v} + p \right) \Delta v \right\}_{i+l_2}^{n+l_2} = \sigma \left\{ u_{i+1}^{k+1} \left(\phi_{i+1+l_2} - \phi_{i+l_2} \right) \right. \\
 & \left. - u_i^{k+1} \left(\phi_{i+l_2} - \phi_{i-l_2} \right) \right\}^{n+1} + (1-\sigma) \left\{ u_{i+1} \left(\phi_{i+1+l_2} - \phi_{i+l_2} \right) \right. \\
 & \left. - u_i \left(\phi_{i+l_2} - \phi_{i-l_2} \right) \right\}^n \frac{\Delta \epsilon^{n+l_2}}{\Delta \epsilon^{n-l_2}} + k \Delta S_{i+l_2}^{n+l_2} \quad (2.21)
 \end{aligned}$$

where the superscript k denotes the iterative value, and

$$\left(\frac{\Delta \epsilon}{\Delta \phi} \right)_{i+l_2}^{n+l_2} = l_2 \left\{ \left(\frac{\Delta \epsilon}{\Delta \theta} \right)_{i+l_2}^{n+1} + \left(\frac{\Delta \epsilon}{\Delta \theta} \right)_{i+l_2}^n \right\} \left(\frac{\Delta \theta}{\Delta \phi} \right)_{i+l_2}^{n+l_2} \quad (2.22)$$

$$\left(\frac{\Delta \epsilon}{\Delta \theta} \right)_{i+l_2}^{n+1} = w_1 \left(\frac{\Delta \epsilon}{\Delta \theta} (\theta, \epsilon) \right)_{i+l_2}^{n+1} + (1-w_1) \left(\frac{\Delta \epsilon}{\Delta \theta} \right)_{i+l_2}^{k-1} \quad (2.23)$$

$$k \left(\frac{\Delta \epsilon}{\Delta v} \right)_{i+j}^{n+1} = \omega_2 \left\{ k \left(\frac{\Delta \epsilon}{\Delta v} \right)^{n+1} + \left(\frac{\Delta \epsilon}{\Delta \phi} \right)^n \right\}_{i+j} \quad (2.24)$$

$$k \left(\frac{\Delta \epsilon}{\Delta v} \right)_{i+j}^{n+1} = \omega_2 \left(\frac{\Delta \epsilon}{\Delta v} (0, \rho) \right)_{i+j}^{n+1} + (1 - \omega_2)^{k-1} \left(\frac{\Delta \epsilon}{\Delta v} \right)_{i+j}^{n+1} \quad (2.25)$$

$$k p_{i+j}^{n+1} = \omega_3 \left\{ k p^{n+1} + p^n \right\}_{i+j} \quad (2.26)$$

$$k p_{i+j}^{n+1} = \omega_3 \left(p (0, \rho) \right)_{i+j}^{n+1} + (1 - \omega_3)^{k-1} p_{i+j}^{n+1} \quad (2.27)$$

$$u_i^{n+1} = \frac{\Delta c}{3} \left(\frac{-\lambda A}{\lambda x} \right)_i^{n+1} \Delta t^{n+1} \quad (2.28)$$

$$\Delta S_{i+j} = P_{f_{i+j}} \Delta S(t) \quad (2.29)$$

The functions $\frac{\Delta \epsilon}{\Delta \theta} (0, \rho)$, $\frac{\Delta \epsilon}{\Delta v} (0, \rho)$, $p(0, \rho)$ and the ratio $\frac{\Delta \theta}{\Delta \phi}$ are given in section 3.1.

The mean free path at a typical interior interface,

$$\frac{k}{\lambda}_i^{n+1} = \omega_4 \left(\frac{k}{\lambda} (\theta_{i-1+j}, \theta_{i+1+j}, \rho_{i-1+j}, \rho_{i+1+j}) \right)^{n+1} + (1 - \omega_4)^{k-1} \frac{k}{\lambda}_i^{n+1} \quad (2.30)$$

is a weighted average reflective of the conditions near the interface, the details of which are given in section 5.2. The source term consists of a space-dependent part, P_f , often referred to as the power factor, and a time-dependent part, $\Delta S(t)$. Both are discussed in section 2.5.

The weights, w_1 , w_2 , w_3 , and w_4 are used as smoothing parameters to dampen out the discontinuities introduced by linear interpolation within the Equation of State and Opacity tables. A typical value for these weights is $\frac{1}{2}$, although it is to the user's advantage to use a value of unity if the tabular values are smooth or if a continuous function is being used in lieu of the tables. This will usually decrease the number of iterations required for convergence. On the other hand, more dampening may be required at times in order to get convergence at all.

The finite difference equations for the boundary zones are derived assuming that the temperature boundary conditions used are of the form

$$a\phi + b \frac{\partial \phi}{\partial x} = \gamma \quad (2.31)$$

with

$$|a| + |b| \neq 0. \quad (2.32)$$

In terms of the derivative, equation 2.31 becomes

$$\frac{\partial \phi}{\partial x}_0 = \frac{\gamma_0 - a_0 \phi_1}{b_0 - a_0 (x_1 - x_0)/\delta_0} \quad (2.33)$$

$$\frac{\partial \phi}{\partial x}_N = \frac{\gamma_N - a_N \phi_{N-1}}{b_N + a_N (x_N - x_{N-1})/\delta_N} \quad (2.34)$$

at each of the boundaries, respectively, by making use of the following first order approximations for ϕ at the boundaries in conjunction with equation (2.31):

$$\phi_0 = \phi_1 - \frac{\partial \phi}{\partial x}_0 (x_1 - x_0)/\delta_0 \quad \text{and} \quad \phi_N = \phi_{N-1} + \frac{\partial \phi}{\partial x}_N (x_N - x_{N-1})/\delta_N \quad (2.35)$$

If $\delta = \frac{1}{2}$, then it is not exactly correct to speak of ϕ at the boundary for its position is the same distance from the boundary as is the adjacent zone temperature, but in the opposite direction. The technique is often referred to as the introduction of "fictitious mesh points" about the boundary. The scheme most nearly approximates the gradient at the boundary as if there were an additional zone extending out from the boundary whose temperature (flux) and pressure profiles are those as given by equations (2.31) and (2.13). If $\delta = 1$, then the boundary condition is said to apply exactly at the boundary.

The user is required to supply a subroutine to calculate α , β , and γ at each boundary. They are either constants or functions of time and/or thermodynamic variables of the boundary zones. For example, if $\alpha = 1$, $\beta = 0$, and $\gamma = [0(t)]^4$, then, the boundary condition will be a temperature profile. If $\delta = 1$, then this profile is imposed directly upon the boundary interface. This type of boundary condition implies that the boundary zone is adjacent to a reservoir of heat that can supply or absorb energy to or from the boundary zone respectively, yet maintain a predetermined temperature regardless of what the boundary zone or any other zone in the problem does. This boundary condition is often used to facilitate coupling the results of another computer program to this program.

In the same manner, if $\alpha = 0$, $\beta = 1$ and $\gamma = 0$, then no energy will be allowed to cross the boundary. Thus, a perfect insulator at the boundary can be easily specified, or a symmetrical problem can be solved more efficiently by doing only half of it. In other situations, it is

desirable to specify the flux or the rate of energy into the boundary zone. This can be done by setting $\alpha = 0$, $\beta = -\frac{ac}{3} \bar{\lambda}$ and $\gamma = F(t)$ where $F(t)$ is a flux profile. The mean free path, $\bar{\lambda}$, at the boundaries is a function of the boundary temperature and/or boundary zone temperature, and the boundary zone density. Again, the details are deferred to section 5.2.

The derivative expressions given by equations (2.33) and (2.34) are substituted into equation (2.20) to obtain a finite difference approximation to the energy equation for each of the boundary zones. The complete system of equations, one for each zone temperature, forms the tri-diagonal system:

$$\begin{aligned}
 & k \left[\sigma_{\mu_1}^{n+1} + m_{1/2} \left(\frac{\Delta \epsilon}{\Delta \phi} \right)_{1/2}^{n+1/2} - \sigma_{\mu_0}^{n+1} \right] \phi_{1/2}^{k+1, n+1} - \sigma_{\mu_1}^{k, n+1} \phi_{1/2}^{k+1, n+1} = \\
 & m_{1/2} \left(\frac{\Delta \epsilon}{\Delta \phi} \right)_{1/2}^{n+1/2} \phi_{1/2}^n + (1-\sigma) \left[(\mu_0 - \mu_1) \phi_{1/2} + \mu_1 \phi_{1/2} - x_0 \right]^n \frac{\Delta \epsilon}{\Delta t} \frac{n+1/2}{n-1/2} \\
 & - k \left(\frac{\Delta \epsilon}{\Delta v} + p \right)_{1/2}^{n+1/2} \Delta V_{1/2}^{n+1/2} - \sigma_{\chi_0}^{k, n+1} + k_{\Delta S_{1/2}}^{n+1/2} + \Delta S p_0^{n+1/2} \quad (2.36) \\
 & \vdots \\
 & - \sigma_{\mu_1}^{k, n+1} \phi_{1/2}^{k+1, n+1} + \left[\sigma_{\mu_1}^{n+1} + m_{1+1/2} \left(\frac{\Delta \epsilon}{\Delta \phi} \right)_{1+1/2}^{n+1/2} + \sigma_{\mu_{1+1}}^{n+1} \right] \phi_{1+1/2}^{k+1, n+1} \\
 & - \sigma_{\mu_{1+1}}^{k, n+1} \phi_{1+1/2}^{k+1, n+1} = m_{1+1/2} \left(\frac{\Delta \epsilon}{\Delta \phi} \right)_{1+1/2}^{n+1/2} \phi_{1+1/2}^n
 \end{aligned}$$

$$\begin{aligned}
& + (1-\sigma) \left[\mu_1 \phi_{1-\frac{1}{2}} - (\mu_1 + \mu_{1+1}) \phi_{1+\frac{1}{2}} + \mu_{1+1} \phi_{1+\frac{1}{2}} \right]^n \frac{\Delta t^{n+\frac{1}{2}}}{\Delta t^{n-\frac{1}{2}}} \\
& - \left(\frac{\Delta \epsilon}{\Delta v} + p \right)_{1+\frac{1}{2}}^{n+\frac{1}{2}} \Delta V_{1+\frac{1}{2}}^{n+\frac{1}{2}} + k_{1+\frac{1}{2}}^{n+\frac{1}{2}} \Delta S_{1+\frac{1}{2}}^{n+\frac{1}{2}}, \quad (2.37)
\end{aligned}$$

$$\begin{aligned}
& - c_{\mu_{N-1}}^{k, n+1} \phi_{N-1-\frac{1}{2}}^{k+1, n+1} + \left[\phi_{N-1}^{n+1} + m_{N-\frac{1}{2}} \left(\frac{\Delta \epsilon}{\Delta \phi} \right)_{N-\frac{1}{2}}^{n+\frac{1}{2}} + \sigma \mu_N^{n+1} \right] \phi_{N-\frac{1}{2}}^{k+1, n+1} = \\
& m_{N-\frac{1}{2}}^{k, n+1} \left(\frac{\Delta \epsilon}{\Delta \phi} \right)_{N-\frac{1}{2}}^{n+\frac{1}{2}} \phi_{N-\frac{1}{2}}^n + (1-\sigma) \left[\mu_{N-1} \phi_{N-1-\frac{1}{2}} - (\mu_{N-1} + \mu_N) \phi_{N-\frac{1}{2}} + \chi_N \right]^n \frac{\Delta t^{n+\frac{1}{2}}}{\Delta t^{n-\frac{1}{2}}} \\
& - \left(\frac{\Delta \epsilon}{\Delta v} + p \right)_{N-\frac{1}{2}}^{n+\frac{1}{2}} \Delta V_{N-\frac{1}{2}}^{n+\frac{1}{2}} + \sigma \chi_N^{k, n+1} + k_{N-\frac{1}{2}}^{n+\frac{1}{2}} \Delta S_{N-\frac{1}{2}}^{n+\frac{1}{2}} + \Delta S p_N^{n+\frac{1}{2}}, \quad (2.38)
\end{aligned}$$

with

$$k_{\mu_0}^{n+1} = k_{\psi_0}^{n+1} k_{\alpha_0}^{n+1}, \quad (2.39)$$

$$k_{\chi_0}^{n+1} = k_{\psi_0}^{n+1} k_{\gamma_0}^{n+1}, \quad (2.40)$$

$$k_{\psi_0}^{n+1} = \frac{\frac{ac}{3} k_{\lambda_0}^{n+1} A_0^{n+1} \Delta t^{n+\frac{1}{2}}}{k_{\beta_0}^{n+1} - k_{\alpha_0}^{n+1} (x_{\frac{1}{2}}^{n+1} - x_0^{n+1}) / \delta_0}, \quad (2.41)$$

$$k_{\mu_N}^{n+1} = k_{\psi_N}^{n+1} k_{\alpha_N}^{n+1}, \quad (2.42)$$

$$k_{\chi_N}^{n+1} = k_{\psi_N}^{n+1} k_{\gamma_N}^{n+1}, \quad (2.43)$$

$$k_{\psi N}^{n+1} = \frac{\frac{ac}{3} k_{\lambda N}^{n+1} k_{A N}^{n+1} \Delta t^{n+1/2}}{k_{\beta N}^{n+1} + k_{\alpha N}^{n+1} (x_N^{n+1} - x_{N-1/2}^{n+1}) / \delta_N} \quad (2.44)$$

2.4 Implicit Solution for Radiation Diffusion

The solution of the tri-diagonal system represented by equations (2.36), (2.37), and (2.38) is an adaptation of the Gaussian elimination scheme for diagonally dominant systems [3]. Note that when $\sigma=0$, that the ϕ 's can be obtained directly, but this fact is not exploited, and the following scheme is a generalization for all values of σ .

Form the terms

$$X_1 = k \left[\sigma \mu_1^{n+1} + m_{1/2} \left(\frac{\Delta \epsilon}{\Delta \phi} \right)_{1/2}^{n+1/2} - \sigma \mu_0^{n+1} \right]^{-1} \quad (2.45)$$

$$Y_1 = \sigma k \mu_1^{n+1} X_1 \quad (2.46)$$

$$Z_1 = \left\{ m_{1/2} k \left(\frac{\Delta \epsilon}{\Delta \phi} \right)_{1/2}^{n+1/2} \phi_{1/2}^n + (1-\sigma) \left[(\mu_0 - \mu_1) \phi_{1/2} + \mu_1 \phi_{1/2} - x_0 \right] \frac{\Delta t^{n+1/2}}{\Delta t^{n-1/2}} - \left\{ \frac{k}{\left(\frac{\Delta \epsilon}{\Delta v} + p \right)_{1/2}^{n+1/2}} \Delta v_{1/2}^{n+1/2} - \sigma k x_0^{n+1} + k \Delta S_{1/2}^{n+1/2} + \Delta S p_0^{n+1/2} \right\} X_1 \right. \quad (2.47)$$

and

$$X_{i+1} = k \left[\sigma \mu_i^{n+1} (1 - Y_i) + m_{i+1/2} \left(\frac{\Delta \epsilon}{\Delta \phi} \right)_{i+1/2}^{n+1/2} + \sigma \mu_{i+1}^{n+1} \right]^{-1} \quad (2.48)$$

$$Y_{i+1} = \sigma k \mu_{i+1}^{n+1} X_{i+1} \quad (2.49)$$

$$Z_{i+1} = \left\{ m_{i+\frac{1}{2}}^k \left(\frac{\Delta \varepsilon}{\Delta \phi} \right)_{i+\frac{1}{2}}^{n+\frac{1}{2}} \phi_{i+\frac{1}{2}}^n + (1-\sigma) \left[\mu_i \phi_{i-\frac{1}{2}} - (\mu_i + \mu_{i+1}) \phi_{i+\frac{1}{2}} \right. \right. \\ \left. \left. + \mu_{i+1} \phi_{i+\frac{1}{2}} \right] n \frac{\Delta t^{n+\frac{1}{2}}}{\Delta t^{n-\frac{1}{2}}} - k \left(\frac{\Delta \varepsilon}{\Delta v} + p \right)_{i+\frac{1}{2}}^{n+\frac{1}{2}} \Delta v_{i+\frac{1}{2}}^{n+\frac{1}{2}} + k_{S_{i+\frac{1}{2}}}^{n+\frac{1}{2}} + \sigma_{\mu_i}^{k, n+1} Z_i \right\} X_{i+1} \quad (2.50)$$

for $i = 1, 2, 3, \dots, N-2$. Then calculate

$${}^{k+1}\phi_{N-\frac{1}{2}}^{n+1} = \left\{ m_{N-\frac{1}{2}}^k \left(\frac{\Delta \varepsilon}{\Delta \phi} \right)_{N-\frac{1}{2}}^{n+\frac{1}{2}} \phi_{N-\frac{1}{2}}^n + (1-\sigma) \left[\mu_{N-1} \phi_{N-1\frac{1}{2}} - (\mu_{N-1} + \mu_N) \phi_{N-\frac{1}{2}} \right. \right. \\ \left. \left. + \chi_N \right] n \frac{\Delta t^{n+\frac{1}{2}}}{\Delta t^{n-\frac{1}{2}}} - k \left(\frac{\Delta \varepsilon}{\Delta v} + p \right)_{N+\frac{1}{2}}^{n+\frac{1}{2}} \Delta v_{N+\frac{1}{2}}^{n+\frac{1}{2}} + \sigma_{\chi_N}^{k, n+1} + k_{S_{N-\frac{1}{2}}}^{n+\frac{1}{2}} + \Delta S p_N^{n+\frac{1}{2}} \right. \\ \left. + \sigma_{\mu_{N-1}}^{k, n+1} Z_{N-1} \right\} \left\{ \sigma_{\mu_{N-1}}^{k, n+1} (1-\gamma_{N-1}) + m_{N-\frac{1}{2}}^k \left(\frac{\Delta \varepsilon}{\Delta \phi} \right)_{N-\frac{1}{2}}^{n+\frac{1}{2}} + \sigma_{\mu_N}^{k, n+1} \right\}^{-1} \quad (2.51)$$

and

$${}^{k+1}\phi_{i+\frac{1}{2}}^{n+1} = \gamma_i {}^{k+1}\phi_{i+\frac{1}{2}}^{n+1} + Z_i \quad (2.52)$$

for $i = N-2, N-3, \dots, 2, 1, 0$.

2.5 Time Advancement Procedure

Figure 3 is a simplified flow chart which illustrates the order in which the combined hydrodynamic and radiation diffusion calculations are done during one time step. Note that the hydrodynamic calculations are done first and are based upon the pressures from the previous time step. The radiation diffusion calculations are then done using the new volumes resulting from a change in position and length of the respective mass zones.

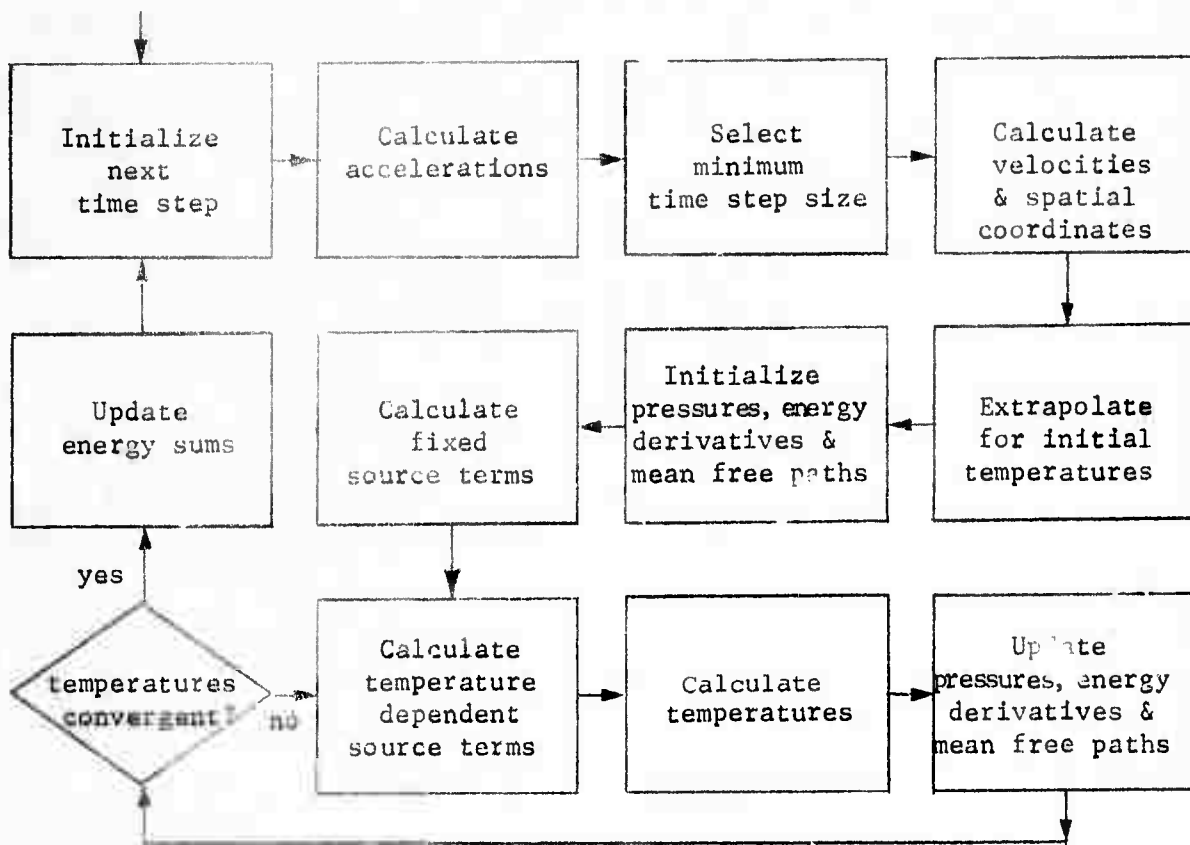


Figure 3

The time step size is determined by a set of user controlled stability and accuracy criteria, one of which is dependent upon the accelerations. Chapter 4 is devoted completely to a discussion of these time step restrictions and the procedure used to determine the optimum time step increment for the current stability requirements and the degree of resolution and accuracy desired.

Subsequent to selecting the time step size and calculating the new spatial dimensions, an extrapolation scheme is introduced to provide initial temperature estimates. Its purpose is to reduce the number of iterations through a linear projection of the previous temperature change:

$$\theta_{i+\frac{1}{2}}^{n+1} = v \frac{\Delta t^{i+\frac{1}{2}}}{\Delta t^{n-\frac{1}{2}}} \left(\theta_{i+\frac{1}{2}}^n - \theta_{i+\frac{1}{2}}^{n-1} \right) + \theta_{i+\frac{1}{2}}^n \quad (2.53)$$

The extrapolation parameter v will typically vary between 0 and 1 with 0, $\frac{1}{2}$ and 1 being the more popular values. Further comments with examples are given in section 7.1 with respect to its use.

Given an initial temperature estimate, the quantities

$$\left(\frac{\Delta \epsilon}{\Delta \theta} \right)_{i+\frac{1}{2}}^{n+1} = \left(\frac{\Delta \epsilon}{\Delta \theta} (\theta, \rho) \right)_{i+\frac{1}{2}}^{n+1} \quad (2.54)$$

$$\left(\frac{\Delta \epsilon}{\Delta v} \right)_{i+\frac{1}{2}}^{n+1} = \left(\frac{\Delta \epsilon}{\Delta \theta} (\theta, \rho) \right)_{i+\frac{1}{2}}^{n+1} \quad (2.55)$$

$$p_{i+\frac{1}{2}}^{n+1} = \left(F(\theta, \rho) \right)_{i+\frac{1}{2}}^{n+1} \quad (2.56)$$

are then calculated for each zone in the normal manner without any smoothing parameters. Likewise, at the interfaces

$$O_{\lambda_0}^{n+1} = \left[\lambda(\theta_0, \phi_{1/2}, \rho_{1/2}) \right]^{n+1}, \quad (2.57)$$

$$O_{\lambda_i}^{n+1} = \left[\lambda(\theta_{i-1/2}, \phi_{i+1/2}, \rho_{i-1/2}, \rho_{i+1/2}) \right]^{n+1} \text{ for } i=1, \dots, N-1, \text{ and} \quad (2.58)$$

$$O_{\lambda_N}^{n+1} = \left[\lambda(\theta_N, \phi_{N-1/2}, \rho_{N-1/2}) \right]^{n+1}. \quad (2.59)$$

All initial values, except the source terms, are now available to start the iterative process for radiation diffusion. The calculation for the source terms is complicated since there are four ways of introducing energy into the problem. Two have been discussed, the imposition of boundary temperature (flux) and pressure profiles. Note that the boundary temperature or flux profiles do not directly result in a source term calculation. In this case, the energy transfer is implicitly included in the energy equation. However, the net flow of energy across the boundaries due to the imposition of temperature and/or flux profiles is simply:

$$\Delta S_{\theta_0}^{n+1/2} = \sigma \left[\mu_0 \phi_{1/2} - x_0 \right]^{n+1} + (1-\sigma) \left[\mu_0 \phi_{1/2} - x_0 \right]^n \frac{\Delta t^{n+1/2}}{\Delta t^{n-1/2}}, \quad (2.60)$$

$$\Delta S_{\theta_N}^{n+1/2} = \sigma \left[x_N - \mu_N \phi_{N-1/2} \right]^{n+1} + (1-\sigma) \left[x_N - \mu_N \phi_{N-1/2} \right]^n \frac{\Delta t^{n+1/2}}{\Delta t^{n-1/2}}, \quad (2.61)$$

The other two source term forms are discussed in chapter 6.

The process iterates as shown in figure 3 until the temperatures converge to a stable value. That is until for each zone

$$\left| \frac{k_{\theta}^{n+1} - k_{\theta}^{n+1}}{k_{\theta}^{n+1}} \right| \leq \epsilon, \quad (2.62)$$

given some user specified epsilon. Since convergence is not guaranteed there is an upper limit upon the number of so called temperature iterations. Twenty is a nominal maximum number of iterations, but the number may be altered by the user to fit his problem. In particular, the limit may be set to unity, reducing the calculations to a non-iterative procedure. The user may also reduce the time step size if the number of iterations per time step becomes excessive or if the temperatures do not converge below the specified epsilon of convergence. In addition to the time step size restriction parameters, several of the other averaging, smoothing and extrapolating parameters discussed above affect the rate of convergence and the number of iterations required for convergence. The ability to change these parameters dynamically make it possible to give the user the answers he desires in a most optimum way. It very often provides the only means of getting past a particularly difficult part of the problem. It also provides the means of getting over particularly stable portions without excessive computer time. Thus, the program need not run always with these parameters set at worst case levels.

The last step in the time advancement scheme is the updating of the energy terms. These terms are calculated and displayed as a means of keeping track of energy conservation. Thus, the following total and partial sums are maintained:

$$IE^{n+1} = \sum_n \sum_i m_{i+1/2} \left[\frac{\Delta \phi}{\Delta \theta} \Delta \theta + \frac{\Delta \phi}{\Delta v} \Delta v \right]_{i+1/2}^{n+1/2} \quad (2.63)$$

$$KE^{n+1} = \frac{1}{2} \sum_i m_{i+1/2} \left[\dot{x}_i^2 + \dot{x}_{i+1}^2 \right]^{n+1/2} \quad (2.64)$$

$$SE^{n+1} = \sum_n \sum_i \Delta S_{i+1/2}^{n+1/2} + \Delta S_{p0}^{n+1/2} + \Delta S_{pN}^{n+1/2} + \Delta S_{e0}^{n+1/2} + \Delta S_{eN}^{n+1/2} \quad (2.65)$$

For energy conservation, it should be the case at all times that

$$IE^{n+1} + KE^{n+1} = SE^{n+1} \quad (2.66)$$

This will never be the case, however. Just due to normal truncation and roundoff errors within the computer, these sums are predestined to not add up correctly. It is the relative difference which is important for the user to monitor. He can effect control over this difference primarily through the convergence parameter and the time step restriction factors as given in chapter 4. The energy conservation and computer time are very real trade-offs. It has been my experience that tight energy conservation will not always give significantly different results. It seems to be important only at certain times within the problem. Many of these are known a priori with respect to, say, the characteristics of the users energy-time profile imposed upon a boundary or a set of zones. In the main however, the user will only tighten-up certain parameters as the need arises.

3.

AREA, VOLUME AND CENTER OF MASS CALCULATIONS

After the acceleration, velocity and space terms are advanced in time, new zone volumes are calculated in order to determine the changes in specific volume over the same time interval. These changes are indicative of the amount of energy converted into kinetic energy due to pressure gradients. Indeed, it is of great importance to monitor the amount of energy converted and its rate of conversion into or from kinetic energy. This energy appears as shocks or shock waves and their characteristic pressure peaks can be dynamically displayed upon a CRT terminal. The user is then able to monitor the motion, distribution and effects of such shocks in direct relation with concurrent displays of temperature and density terms. Of special interest are the changes in volume at the problem boundaries. It is here that external forces, in the form of boundary pressures, pump kinetic energy into or out of the problem. In addition, the motion of zone boundaries requires that new zone mass centers must be calculated from which finite difference terms can be formed to describe the transport of energy from one zone to the next by the diffusion of radiation.

The purpose of this chapter is to give the computational details used for determining the volume and mass centers for each zone. Each of the three geometries is discussed.

3.1 Plane Geometry

In plane geometry, the space dependent radius adds to the complexity of the area, volume and center of mass determinations. First,

let me point out that the center of mass we wish to determine is not (in general) equivalent to the center of gravity. Instead, it is the point on the axis which divides the zone in half with respect to its volume and consequently its mass since it is assumed to have a uniform density. Secondly, note that equations (2.7) and (5.36) require such a division.

Unfortunately, time has not allowed an exact division for the case in which the radii changes linearly with respect to space. Instead, the center of gravity was calculated as an approximation for the center of these sections. I refer to such sections as truncated frustrums or trapezoids of revolution.

The user must provide a description of the container. This is done independently of the initial spatial description of the material within in the form of a space profile of radii and space pairs

$$(r_{p_j}, x_{p_j}), j = 1, 2, \dots, J+1, \quad (3.1)$$

such that

$$x_{p_j} \leq x_{p_{j+1}}, \quad (3.2)$$

$$\text{and } r_{p_j} > 0. \quad (3.3)$$

The volume of a zone delimited by interfaces at x_1^n and x_{i+1}^n at some time $t = t^n$ is then given by

$$V_{i+1}^n = \sum_{k=j,i} V_k^n, \quad (3.4)$$

with

$$V_k^n = \pi \Delta x_k^n \xi_k^n, \quad (3.5)$$

$$\Delta x_j^n = x_{p_j}^n - x_1^n, \quad (3.6)$$

$$\Delta x_k^n = x_{p_k}^n - x_{p_{k-1}}^n \quad \text{for } k = j+1, \dots, l-1 \quad (3.7)$$

$$\Delta x_l^n = x_{i+1}^n - x_{p_{l-1}}^n, \quad (3.8)$$

$$\xi_j^n = \begin{cases} (r_1^n)^2 & \text{if } r_{p_{j-1}} = r_{p_j}, \\ 1/3 \left[(r_1^n)^2 + r_1^n r_{p_j} + (r_{p_j})^2 \right] & \text{if } r_{p_{j-1}} \neq r_{p_j}, \end{cases} \quad (3.9)$$

$$\xi_k^n = \begin{cases} (r_{p_{k-1}})^2 & \text{if } r_{p_{k-1}} = r_{p_k}, \\ 1/3 \left[(r_{p_{k-1}})^2 + r_{p_{k-1}} r_{p_k} + (r_{p_k})^2 \right] & \text{if } r_{p_{k-1}} \neq r_{p_k} \end{cases} \quad (3.10)$$

for $k = j+1, \dots, l-1$ and

$$\xi_l^n = \begin{cases} (r_{p_{l-1}})^2 & \text{if } r_{p_{l-1}} = r_{p_l}, \\ 1/3 \left[(r_{p_{l-1}})^2 + r_{p_{l-1}} r_{p_l} + (r_{p_l})^2 \right] & \text{if } r_{p_{l-1}} \neq r_{p_l} \end{cases} \quad (3.11)$$

where

$$x_{p_{j-1}}^n \leq x_1^n < x_{p_j}^n, \quad x_{p_{l-1}}^n < x_{i+1}^n \leq x_{p_l}^n \quad (3.12)$$

for some j and l , $1 < j \leq l \leq J$.

In the special (and most often encountered) case for which

$$x_{p_{j-1}}^n \leq x_1^n < x_{i+1}^n \leq x_{p_j}^n, \quad (3.13)$$

then

$$v_{i+j}^n = \Delta x_{i+j} \xi_j^n, \quad (3.14)$$

where

$$\xi_j^n = \begin{cases} (r_i^n)^2 & \text{for } r_i^n = r_{i+1}^n, \\ 1/3 \left[(r_i^n)^2 + r_i^n r_{i+1}^n + (r_{i+1}^n)^2 \right] & \text{for } r_i^n \neq r_{i+1}^n. \end{cases} \quad (3.15)$$

In both cases,

$$r_i^n = (x_i^n - x_{p_{j-1}}) \frac{(r_{p_j} - r_{p_{j-1}})}{(x_{p_j} - x_{p_{j-1}})} + r_{p_{j-1}}. \quad (3.16)$$

If the restrictions given above in equations (3.12) or (3.13) cannot be satisfied because part or all of the zone lies outside of the pipe profile, then the formula above is used equally well to extrapolate for the interface radii. In these cases, either equation (3.4) or (3.14) apply depending upon whether more than one (the last) pipe section is involved. Care must be taken to insure that $r_i^n > 0$ for all $i = 1, \dots, N$.

The zone center is then given by

$$x_{i+j} = \frac{\sum_{k=j,i} \bar{x}_k^n v_k^n}{\sum_{k=j,i} v_k^n}, \quad (3.17)$$

with

$$\bar{x}_j^n = \begin{cases} \frac{1}{2}(x_{p_j} + x_i^n) & \text{if } r_{p_{j-1}} = r_{f_j}, \\ \frac{\pi(\Delta x_j)^2 \left[3 \xi_j^n + r_i r_{i+1} + 2(r_{p_j})^2 \right]}{12 v_j^n} + x_i^n & \text{if } r_{p_{j-1}} = r_{p_j}, \end{cases} \quad (3.18)$$

$$\bar{x}_k^n = \begin{cases} \frac{1}{2}(x_{p_k}^n - x_{p_{k-1}}^n) & \text{if } r_{p_{k-1}} = r_{p_k}, \\ \frac{\pi(\Delta x_j)^2 \left[3 \xi_k^n + r_{p_{k-1}} r_{p_k} + 2(r_{p_k})^2 \right]}{12V_k^n} & \text{if } r_{p_{k-1}} \neq r_{p_k}, \end{cases} \quad (3.19)$$

for $k = j+1, \dots, l-1$ and

$$\bar{x}_l^n = \begin{cases} \frac{1}{2}(x_{p_{l+1}}^n - x_{p_l}^n) & \text{if } r_{p_{l+1}} = r_{p_l}, \\ \frac{\pi(\Delta x_{l-1})^2 \left[3 \xi_l^n + r_{p_{l-1}} r_{p_l} + (r_{p_l})^2 \right]}{12V_l^n} & \text{if } r_{p_{l-1}} \neq r_{p_l}, \end{cases} \quad (3.20)$$

or if (3.13) applies,

$$\bar{x}_{1+j}^n = \begin{cases} \frac{1}{2}(x_{1+j}^n + x_1^n) & \text{if } r_1^n = r_{1+j}^n, \\ \frac{\pi(\Delta x_{1+j})^2 \left[(r_1^n)^2 + 2r_1^n r_{1+j}^n + 3(r_{1+j}^n)^2 \right]}{12V_{1+j}^n} & \text{if } r_1^n \neq r_{1+j}^n, \end{cases} \quad (3.21)$$

if restriction (3.13) applies.

The area of a typical interface is simply

$$A_j^n = \pi(r_1^n)^2. \quad (3.22)$$

3.2 Cylindrical and Spherical Geometry

The calculations for cylindrical and spherical geometry are much simpler than that for plane geometry for there is no analog to the flexible cross section allowed therein.

For cylindrical geometry

$$A_1^n = 2\pi x_1^n h, \quad (3.23)$$

$$V_{1+1/2}^n = \pi \left[(x_{1+1}^n)^2 - (x_1^n)^2 \right] h, \quad (3.24)$$

and

$$x_{1+1/2}^n = \left\{ \frac{1}{2} \left[(x_{1+1}^n)^2 + (x_1^n)^2 \right] \right\}^{1/2} \quad (3.25)$$

where h is the height of the cylinder as supplied by the user.

For spherical geometry

$$A_j^n = 4\pi (x_1^n)^2, \quad (3.26)$$

$$V_{1+1/2}^n = 4/3\pi \left[(x_{1+1}^n)^3 - (x_1^n)^3 \right], \quad (3.27)$$

and

$$x_{1+1/2}^n = \left\{ \frac{1}{2} \left[(x_{1+1}^n)^3 + (x_1^n)^3 \right] \right\}^{1/3}. \quad (3.28)$$

3.3 Change in Volume at the Boundaries

As required in equations (2.16) and (2.17), the change in volume at each boundary is calculated in a manner not unlike that given above. Since the boundary volume element is regarded as a change in volume, the sense or sign of the change is important. Note that the volume at boundary $i = 0$ must be calculated over the interval from x_0^n to x_0^{n+1} . If $x_0^{n+1} < x_0^n$, then the interval is thought of as having a negative length in order to determine the correct sign of $\Delta V_0^{n+1/2}$. The same care and consideration is given to the other boundary. Note that if $\Delta V_0^{n+1/2} > 0$ and/or $\Delta V_n^{n+1/2} < 0$, then work is done on the system.

4.

TIME STEP SIZE DETERMINATION

A number of restrictions are placed upon the time step size for purposes of stability, resolution and convenience. Each is discussed in detail with respect to their effect upon the solution and each is controlled directly or indirectly through user specified parameters.

4.1 Courant-Friedrichs-Levy Hydrodynamic Stability

Criterion [3]:

$$\Delta t^{n+1/2} \leq \Delta t_c^{n+1/2} = \min_i \left\{ \frac{\Delta x_{i+1/2}^{n+1}}{u_{s,i+1/2}^{n+1}} \right\}. \quad (4.1)$$

This restriction prohibits the shock front moving at a velocity u_s from passing completely through any one zone during the time step. Note that $\Delta x_{i+1/2}^{n+1}$ and $u_{s,i+1/2}^{n+1}$ are not known at the beginning of a time step. The zone width is an explicit function of $\Delta t^{n+1/2}$ and the shock velocity is a function of the resultant pressure and density, the details of which are given in section 5.1, equation (5.25).

The procedure used to determine the Courant time step, therefore, is to estimate an initial value

$$\Delta t_c^{n+1/2} = C_{fac} \min_i \left\{ \frac{\Delta x_{i+1/2}^n}{u_{s,i+1/2}^{n+1}} \right\}, \quad (4.2)$$

with $0 < C_{fac} \leq 1$, and then check after the initial extrapolation and each subsequent iteration that

$$\Delta t^{n+1/2} \leq \Delta t_c^{n+1/2} = \min_i \left\{ \frac{\Delta x_{i+1/2}^{n+1}}{k_{u_{s,i+1/2}^{n+1}}} \right\} \quad (4.3)$$

If at any time during the iterative solution it is found that

$k_{\Delta t_c}^{n+1/2} < \Delta t^{n+1/2}$, then an error message is displayed and the program is put into a waiting mode. The user is then expected to initiate a corrective procedure which will enable the program to continue in a stable condition.

The corrective procedure may be nothing more than reducing the time step size directly or indirectly through the parameter C_{fac} and then backing-up and restarting the current time step. It can, however, involve a detailed examination of the conditions of the offending zone or zones in order to understand the mechanisms creating the instability. More precise solutions may then be directed at the particularly sensitive variables involved.

4.2 Hydrodynamic Zone Increment Change Restriction

$$H_{fac} \geq \max_i \left| 1 - \frac{\Delta x_{i+1/2}^{n+1}}{\Delta x_{i+1/2}^n} \right|. \quad (4.4)$$

This is a restriction on the fractional change in the length of a zone, with $0 < H_{fac} < 1$. Its primary purpose is to minimize the discontinuity in the distance between zones and the volumes of each zone from one time step to the next. It also prevents a complete collapse of a zone, and, in particular, the inversion or crossing of adjacent interfaces. In addition, this restriction eliminates most of the problem of mismatched zones with respect to their mass ratios. The problem arises during a given time step when a massive zone crushes and collapses a much less massive zone before the latter is able to build up a resisting

pressure. Another difficulty with adjacent zones of widely differing masses occurs when an average opacity is calculated at the interface between the zones. This problem is discussed in detail in chapter 5.

A time step increment satisfying the restriction given by (4.4) can be explicitly calculated once the acceleration terms are known since

$$\begin{aligned}
 \Delta x_{i+1/2}^{n+1} &= x_{i+1}^{n+1} - x_i^{n+1} \\
 &= x_{i+1}^n - x_i^n \\
 &\quad + (\ddot{x}_{i+1}^{n-1/2} - \ddot{x}_i^{n-1/2}) \Delta t^{n+1/2} \\
 &\quad + (\ddot{x}_{i+1}^n - \ddot{x}_i^n) \Delta t^{n+1/2} \frac{(\Delta t^{n+1/2} + \Delta t^{n-1/2})}{2}
 \end{aligned} \tag{4.5}$$

using equations (2.8) and (2.9). Thus, a maximum value of $t^{n+1/2}$ needs to be found such that

$$|a_i (\Delta t^{n+1/2})^2 + b_i \Delta t^{n+1/2}| \leq c_i, \tag{4.6}$$

where

$$a_i = \frac{1}{2}(\ddot{x}_i^n - \ddot{x}_{i+1}^n), \tag{4.7}$$

$$b_i = a_i \Delta t^{n-1/2} + (\ddot{x}_i^{n-1/2} - \ddot{x}_{i+1}^{n-1/2}), \tag{4.8}$$

$$c_i = H_{\text{fac}} \Delta x_{i+1/2}^n, \tag{4.9}$$

for $i = 0, 1, \dots, N-1$. A solution, $\Delta t_h^{n+1/2}$, of the system represented by (4.6) is in general a quadratic root depending upon the values of the coefficients a_i , b_i and c_i . Since $c_i > 0$, it is possible to show that

$$\Delta t_h^{n+1/2} = \min_i \begin{cases} \infty & \text{if } a_i = b_i = 0 \\ c_i / |b_i| & \text{if } a_i = 0, b_i \neq 0 \\ \frac{-b_i + (b_i^2 + 4a_i c_i)^{1/2}}{2a_i} & \text{if } \begin{cases} a_i > 0, b_i \geq 0 \\ a_i > 0, b_i < 0, b_i^2 - 4a_i c_i < 0 \\ a_i < 0, b_i > 0, b_i^2 + 4a_i c_i \geq 0 \end{cases} \\ \frac{-b_i - (b_i^2 - 4a_i c_i)^{1/2}}{2a_i} & \text{if } \begin{cases} a_i > 0, b_i < 0, b_i^2 - 4a_i c_i \geq 0 \\ a_i < 0, b_i > 0, b_i^2 + 4a_i c_i < 0 \\ a_i < 0, b_i \leq 0 \end{cases} \end{cases} \quad (4.10)$$

The user can dynamically change the importance of this restriction through the parameter H_{fac} , rezoning if necessary when the restriction is too greatly localized at one zone.

4.3 Temperature Change Restriction

$$\Delta t^{n+1/2} \leq \Delta t_{\theta}^{n+1/2} = T_{fac} \min_i \left\{ \frac{\theta_{i+1/2}^n + \theta_p}{|\theta_{i+1/2}^n - \theta_{i+1/2}^{n-1}|} \right\} \Delta t^{n-1/2}. \quad (4.11)$$

This restriction, not unlike the others, is added to reduce the truncation error and give better resolution and accuracy when desired. Usually, $0 < T_{fac} \leq 1$, and the parameter θ_p is a reference or base temperature above which the restriction is to be applied. Both parameters may be set dynamically by the user to best suit his requirements at any time throughout the solution of his problem.

Specifically, an economic trade-off with computer time consumption per unit of problem time can be made at those points when the temperature and pressure gradients are such that a first order approximation remains

valid over a much larger time interval. Note that the three time step restrictions discussed up to this point will automatically increase or decrease the time step increment depending upon current conditions internal to the problem. The user, however, has control over the degree to which these restrictions will be applied.

If

$$\frac{\Delta \epsilon^{n-1/2}}{\Delta \phi^{1+1/2}} < \epsilon_3 \approx 0, \quad (4.12)$$

meaning that the temperature change occurs irrespective of the specific heat of the zone, then the temperature change restriction on that zone is ignored.

4.4 Doubling Restriction

$$\Delta t^{n+1/2} \leq \Delta t_d^{n+1/2} = 2 \Delta t^{n-1/2}. \quad (4.13)$$

This arbitrary restriction prevents the time step size from becoming too large too fast. If the next time step is quite large with respect to the previous one, corresponding changes in the derivatives, pressure, opacity, etc., may be too large to calculate accurately even in light of the iterative scheme. A rapidly varying time step from one time step to another can adversely effect the hydrodynamics through equation (2.8). Note that there is no restriction upon how small a time step can become even with respect to the previous time step size.

4.5 Print Restriction

$$\Delta t^{n+1/2} \leq \Delta t_p^{n+1/2} = t_{prt} - t^n. \quad (4.14)$$

At user specified intervals, the program prints out the current space coordinates, temperatures, pressures, etc., so that a permanent record of the problem solution may be retained for further study at a later time. The program also makes a hard copy of the image on the display and writes out onto a user file the current state of the program so that it may be restarted at that time if so desired at some later time. This dump feature allows the user to run a problem at several sittings, restarting at or near the point in time at which he stopped previously. It also facilitates his going back in time and trying a different solution path by changing one or more program parameters or variables.

The specific print-plot-dump times are given during the input phase of the program in the form of a print profile. The profile consists of a sequence $(\Delta t_{prt_j}, t_{prt_j})$. The next scheduled print time,

$$t_{prt} = t_{prt_j} + m\Delta t_{prt_j}, \quad (4.15)$$

is determined by the j and the m for which

$$(m-1)\Delta t_{prt_j} \leq t^n - t_{prt_j} < m\Delta t_{prt_j} \quad (4.16)$$

and

$$t^n < t_{prt_{j+1}} \quad (4.17)$$

if there is a next value $t_{\text{prt}_{j+1}}$. Also, if

$$t_{\text{prt}_{j+1}} \leq t_{\text{prt}_j} + m\Delta t_{\text{prt}_j}, \quad (4.18)$$

then t_{prt} is set to $t_{\text{prt}_{j+1}}$, and the index j is advanced by one.

The print profile is used to obtain print-outs over certain intervals of interest at "nice" values of time, usually factors of two and five. Both the profile and the next scheduled print time may be altered dynamically.

Since the print times will normally interrupt the running sequence with a short time step, the program attempts to restore the time step size for the next time advancement to the level at which it had been running. Specifically, the temperature change and doubling restrictions will use $\Delta t^{n-1/2}$ as a guide in lieu of $\Delta t^{n-1/2}$. The other restriction criterion are used as stated after a print cycle.

4.6 Maximum Restriction

$$\Delta t^{n+1/2} \leq \min(\Delta t_m, \Delta t_s). \quad (4.19)$$

Once in a while it is convenient to set a limit on the size of the time step. It is particularly helpful when the user is attempting to follow a phenomenon which is not being controlled automatically by any of the other time step limiting procedures.

A one time only maximum may be set through Δt_s . It is automatically reset to infinity for the next time step. There is an automatic back-up scheme which may occur if the temperatures don't converge. When this back-up occurs, Δt_s is set to one half the value of $\Delta t^{n+1/2}$ and the calculations for that time step are restarted. An overall maximum Δt_m may be set and remains as set until reset.

Note that while $\Delta t^{n+1/2}$ may be altered directly by user, it is not effective unless he also schedules a back-up since $\Delta t^{n+1/2}$ is recomputed at the beginning of the next time step. The back-up procedure does not restart the time step calculations at the beginning of the advancement procedure as illustrated in Figure 3, but instead, restarts with the selection of the time step size. The accelerations and previously discussed time step size restrictions remain valid during a back-up.

4.7 Hold Time Restriction

$$\Delta t^{n+1} \leq \Delta t_w^{n+1/2} = t_w - t^n \quad (4.20)$$

It is often useful to set a time t_w at which the user wishes to put the program in a hold or wait condition. This feature insures that he will be able to put into effect changes at certain specified problem times crucial to the overall problem solution.

If $t_w < t^n$, then the restriction does not hold and the program automatically sets Δt_w to the machine relative infinity.

4.8 Time Step Size Selection

The time step size selected is simply:

$$\Delta t^{n+1/2} = \min \left\{ \Delta t_c, \Delta t_h, \Delta t_\theta, \Delta t_d, \Delta t_p, \Delta t_m, \Delta t_s, \Delta t_w \right\}^{n+1/2} . \quad (4.21)$$

5.

MATERIAL PROPERTIES

Equation of state and opacity data must be provided for each specified material. These data are available in tabular form on a mass storage device and are automatically read into the program when called for by name during the input phase. The user may also include his own special purpose tables or routines. Sometimes the material properties can be calculated from a set of parameterized equations. This may be the case when a problem is run for which there is an analytical solution to check with.

This chapter will limit its discussion to the standard material property tables and the procedures which are used to calculate the required thermodynamic quantities.

5.1 Equation of State

The gaseous equation of state tables are organized by density and temperature within each material type. For each tabular density in the form $\ln v_j$, there is a sequence of temperature, internal energy and proportionality triplets, $(\theta, e_g, b')_{j,k}$, such that:

$$p_g = \frac{b'\theta}{v}, \quad (5.1)$$

$$\ln v_1 < \ln v_2 < \dots < \ln v_j, \quad (5.2)$$

$$\theta_{j,1} < \theta_{j,2} < \dots < \theta_{j,k}, \quad (5.3)$$

with $J, K \geq 1$. Note that there is no requirement that the tables be the same size from one material type to another, or that $\theta_{j,k} = \theta_{j+1,k}$ for any j, k within the table. A typical maximum table size would be $J = 20$ and $K = 30$.

The material internal energy, ϵ_g , includes the kinetic energy of the free particles; the dissociation, ionization, and excitation energy; but not the radiation energy given by

$$\epsilon_r = a\phi v. \quad (5.4)$$

The equation of state tables are generated by other computer programs [4], and there are many tables in existence for the common elements, compounds and mixtures.

Given some temperature and density, (θ, ρ) , the energy derivatives and proportionality constant are approximated from these tables through the following interpolation formulae:

$$\begin{aligned} \frac{\Delta \epsilon}{\Delta \theta} (\theta, \rho) = & \frac{\ln v - \ln v_j}{\ln v_{j+1} - \ln v_j} \left\{ \frac{\epsilon_{j+1, l+1} - \epsilon_{j+1, l}}{\theta_{j+1, l+1} - \theta_{j, l}} - \frac{\epsilon_{j, k+1} - \epsilon_{j, k}}{\theta_{j, k+1} - \theta_{j, k}} \right\} \\ & + \frac{\epsilon_{j, k+1} - \epsilon_{j, k}}{\theta_{j, k+1} - \theta_{j, k}} + 4a\theta^3 v, \end{aligned} \quad (5.5)$$

$$\begin{aligned} \frac{\Delta \epsilon}{\Delta v} (\theta, \rho) = & \rho \theta^2 \left[\frac{\ln v - \ln v_j}{\ln v_{j+1} - \ln v_j} \left\{ \frac{b'_{j+1, l+1} - b'_{j+1, l}}{\theta_{j+1, l+1} - \theta_{j+1, l}} - \frac{b'_{j, k+1} - b'_{j, k}}{\theta_{j, k+1} - \theta_{j, k}} \right\} \right. \\ & \left. + \frac{b'_{j, k+1} - b'_{j, k}}{\theta_{j, k+1} - \theta_{j, k}} \right] + a\phi, \end{aligned} \quad (5.6)$$

$$b'(\theta, \rho) = \frac{\ln v - \ln v_j}{\ln v_{j+1} - \ln v_j} (b'_{j+1} - b'_j) + b'_j, \quad (5.7)$$

where

$$b'_j = b'_{j, k} + (\theta - \theta_{j, k}) \frac{b'_{j, k+1} - b'_{j, k}}{\theta_{j, k+1} - \theta_{j, k}}, \quad (5.8)$$

$$b'_{j+1} = b'_{j+1,l} + (\theta - \theta_{j+1,l}) \frac{b'_{j+1,l+1} - b'_{j+1,l}}{\theta_{j+1,l+1} - \theta_{j+1,l}}, \quad (5.9)$$

assuming that

$$\ln v_j \leq \ln v \leq \ln v_{j+1} \quad \text{with } 1 \leq j < J, \quad (5.10)$$

$$\theta_{j,k} \leq \theta \leq \theta_{j,k+1} \quad \text{with } 1 \leq k < K, \quad (5.11)$$

$$\theta_{j+1,l} \leq \theta \leq \theta_{j+1,l+1} \quad \text{with } 1 \leq l < K. \quad (5.12)$$

If one or more of the above conditions given by (5.10), (5.11) and (5.12) do not hold, then equations (5.5), (5.6), (5.7), (5.8) and (5.9) are used as extrapolation formulae. The evils of this extrapolation scheme have shown up often upon the graphics scope in the form of non-convergence and discontinuity in successive values. It is hoped that through the graphics monitor, a new extrapolation scheme or limits upon the existing scheme can be established which will aid the user in bringing his problem up to those temperatures and densities which are within the bounds of the tables. The user must often compromise with storage limitations and put in tables which cover only a particular area of interest with respect to temperature and density.

Equation (5.5) gives an approximation for $\frac{\partial \epsilon}{\partial \theta}$, the specific heat. The tables are constructed for linear interpolation on θ ; therefore, equation (5.5) in terms of ϕ is unsatisfactory for an approximation to $\frac{\partial \epsilon}{\partial \phi}$. An acceptable scheme makes use of the relation

$$\frac{\partial \epsilon}{\partial \phi} = \frac{\partial \epsilon}{\partial \theta} \frac{\partial \theta}{\partial \phi}. \quad (5.13)$$

with

$$\frac{\partial \theta}{\partial \phi} \approx \frac{\Delta \theta}{\Delta \phi} . \quad (5.14)$$

Therefore,

$$k \left(\frac{\Delta \epsilon}{\Delta \phi}(\theta, \rho) \right)_{i+j}^{n+j} = k \left(\frac{\Delta \epsilon}{\Delta \theta}(\theta, \rho) \right)_{i+j}^{n+j} k \left(\frac{\Delta \theta}{\Delta \phi} \right)_{i+j}^{n+j} , \quad (5.15)$$

where

$$k \left(\frac{\Delta \theta}{\Delta \phi} \right)_{i+j}^{n+j} = \frac{k_{\theta}^{n+1} - \theta_{i+j}^n}{k_{\phi}^{n+1} - \phi_{i+j}^n} = \frac{1}{(k_{\theta}^{n+1} + \theta_{i+j}^n) ([k_{\theta}^{n+1}]^2 + [\theta_{i+j}^n]^2)} \quad (5.16)$$

Note that this approximation avoids problems with loss of significance between nearly equal quantities and division by zero (within the computer's finite resolution).

Equation (5.6) is derived using the thermodynamic relationship

$$\frac{\partial \epsilon}{\partial v} = \theta \frac{\partial p}{\partial \theta} - p, \quad (5.17)$$

in conjunction with equation (5.1). A more direct form would be

$$\frac{\Delta \epsilon}{\Delta v}(\theta, \rho) = \frac{\epsilon_{j+1} - \epsilon_j}{\ln v_{j+1} - \ln v_j} \frac{\rho_{j+1} + \rho_j}{2} + a\phi, \quad (5.18)$$

where

$$\frac{\Delta(\ln v)}{\Delta v} \approx \frac{1}{v} = \rho, \quad (5.19)$$

$$\epsilon_{g_j} = \epsilon_{g_{j,k}} + (\theta - \theta_{j,k}) \frac{\epsilon_{g_{j,k+1}} - \epsilon_{g_{j,k}}}{\theta_{j,k+1} - \theta_{j,k}}, \quad (5.20)$$

$$c_{g_{j+1}} = c_{g_{j+1,l}} + (\theta - \theta_{j+1,l}) \frac{c_{g_{j+1,l+1}} - c_{g_{j+1,l}}}{\theta_{j+1,l+1} - \theta_{j+1,l}}. \quad (5.21)$$

The two forms give different results and the former was chosen only because it proved to be cheaper.

The total pressure is the sum of the gas pressure given by equation (5.1), the radiation pressure,

$$p_r = \frac{a}{3} \phi, \quad (5.22)$$

and the pseudo-viscous pressure, q , which is an artificial aid used to fit the shock in a smooth manner over several zones [3]. Two forms of pseudo-viscous pressure are provided, the choice of which is an option provided to the user. The form linear in the velocity gradient is

$$k_{q_{i+l_2}}^{n+1} = \begin{cases} \eta_1 \rho_{i+l_2}^{n+1} k_{u_{i+l_2}}^{n+1} \left| \dot{x}_{i+1}^{n+l_2} - \dot{x}_i^{n+l_2} \left(\frac{x_1^{n+1}}{x_{i+1}^{n+1}} \right)^\alpha \right| & \text{for } \Delta v_{i+l_2}^{n+l_2} < 0, \\ 0 & \text{for } \Delta v_{i+l_2}^{n+l_2} \geq 0, \end{cases} \quad (5.23)$$

and the quadratic form is

$$k_{q_{i+l_2}}^{n+1} = \begin{cases} \eta_2 \rho_{i+l_2}^{n+1} \left[\dot{x}_{i+1}^{n+l_2} - \dot{x}_i^{n+l_2} \left(\frac{x_1^{n+1}}{x_{i+1}^{n+1}} \right)^\alpha \right]^2 & \text{for } \Delta v_{i+l_2}^{n+l_2} < 0, \\ 0 & \text{for } \Delta v_{i+l_2}^{n+l_2} \geq 0, \end{cases} \quad (5.24)$$

Both η_1 and η_2 may be altered by the user at any time through the keyboard and are initially set at 0.8 and 1.0 respectively. The parameter $\alpha=0,1,2$ for plane, cylindrical and spherical geometry respectively. The sonic velocity is given by

$$k_{u_{i+l_2}}^{n+1} = 4/3 \left[k_{p_{i+l_2}}^{n+1} v_{i+l_2}^{n+1} \right]^{1/2}. \quad (5.25)$$

Note that the sonic velocity is a function of the total pressure and is, therefore, one iteration behind. In summary, the total pressure is given by the sum

$$k \left(p(\theta, \rho) \right)_{i+1/2}^{n+1/2} = \left(p_g + p_r + \eta \right)_{i+1/2}^{n+1/2}. \quad (5.26)$$

5.2 Mean Free Path

Corresponding to a conductivity coefficient in thermal diffusion programs, a dimensionally equivalent coefficient, $\frac{ac}{3} \bar{\lambda}$, is calculated for use in the radiation diffusion term of equation (2.6). The mean free path, $\bar{\lambda}$, is a function of both temperature and density as were the preceding energy and pressure terms. It is calculated using the relation

$$\bar{\lambda} = \frac{1}{\kappa \rho} \quad (5.27)$$

where κ , the opacity, is typically calculated through the interpolation of tables given in terms of density and temperature. The scheme is further complicated due to the requirement that we must obtain a value for $\bar{\lambda}$ at the interface while the temperature and density values are available only at the zone mid-points. Many schemes have been tried and tested [5, 6] in a number of similar computer programs.

The scheme implemented here expands upon ideas developed in the FF program [5]. The central idea is to try to get a better estimate of local conditions at the interface and then calculate a mean free path based upon these conditions.

Of prime importance was an interface temperature since the density changes from one time step to the next tend to be overshadowed by much greater changes in temperature. Also, the opacity tends to be a much

less sensitive function of density. Thus, density effects were somewhat ignored with emphasis upon arriving at a suitable interface temperature.

Note that the radiation energy equation

$$E_r = a\theta^4 V \quad (5.28)$$

implies that $\phi = \theta^4$ is a measure of the energy in a zone (as far as radiation transport is concerned). This assumption is valid only if ϕ represents the whole zone. The temperature point is, therefore, located at the mass center rather than the spatial center of the zone. This also agrees with the hydrodynamic differencing as explained in section 2.2 and given by equation (2.7).

The radiation energy in the volume between mass centers about a typical interface is simply

$$E_{r_1} = \frac{a}{2} \left[(\phi V)_{1-\frac{1}{2}} + (\phi V)_{1+\frac{1}{2}} \right]. \quad (5.29)$$

Also,

$$E_{r_1} = a(\phi V)_1 \quad (5.30)$$

thus,

$$\phi_1 = \frac{(\phi V)_{1-\frac{1}{2}} + (\phi V)_{1+\frac{1}{2}}}{V_{1-\frac{1}{2}} + V_{1+\frac{1}{2}}} \quad (5.31)$$

This temperature is exact. Its position is unknown though and one can only say that it is the best estimate which can be obtained in the neighborhood of interface. In the end, its position is unimportant. What is important is that it provides a means of obtaining the correct flux across the interface agreeing with empirical and analytical results.

Given the interface temperature, an opacity is calculated for each zone in the neighborhood of the interface which is reflective of the respective material type, temperature and density. These values are referred to as κ_1^+ and κ_1^- where

$$\kappa_1^+ = \kappa(\theta_1, \rho_{1+\frac{1}{2}}) \quad (5.32)$$

and

$$\kappa_1^- = \kappa(\theta_1, \rho_{1-\frac{1}{2}}) \quad (5.33)$$

The calculational details of the opacity functions are given in the next section.

Note that the opacity is a measure of the average cross sectional area as seen by a photon. Its units of measure are area per gram of material. The total opacity is, therefore, κm , where m is the mass of the material which has opacity κ . Thus in our case

$$(\kappa m)_1 = \frac{1}{2} \left(\kappa_1^- m_{1-\frac{1}{2}} + \kappa_1^+ m_{1+\frac{1}{2}} \right) \quad (5.34)$$

and since

$$\bar{\lambda}_1 = \left(\frac{V}{\kappa m} \right)_1, \quad (5.35)$$

then

$$\bar{\lambda}_1 = \frac{V_{1-\frac{1}{2}} + V_{1+\frac{1}{2}}}{\kappa_1^- m_{1-\frac{1}{2}} + \kappa_1^+ m_{1+\frac{1}{2}}}. \quad (5.36)$$

Since each zone is assumed to be homogeneous in density, the mass center is also the volume center. Thus, the volume between $x_{1-\frac{1}{2}}$ and x_1 is simply $\frac{1}{2}V_{1-\frac{1}{2}}$. This fact is also used in equation (2.7).

An average flux is then given by

$$F_i = - \frac{ac}{3} \bar{\lambda}_i \left(\frac{\psi_{i+\frac{1}{2}} - \psi_{i-\frac{1}{2}}}{x_{i+\frac{1}{2}} - x_{i-\frac{1}{2}}} \right). \quad (5.37)$$

The spatial position of this flux level is not fixed and is not known.

It becomes important only when the radii varies between $x_{i-\frac{1}{2}}$ and $x_{i+\frac{1}{2}}$.

This flux value is also valid for but a short time. Thus care and consideration must be given to the proper selection of A , the area, and Δt , the time step size, which are used to give

$$\Delta Q_i = F_i A_i \Delta t, \quad (5.38)$$

the net amount of energy transported from one zone to the next by radiation. In this case, the area used is the actual area at x_i . It will in general, vary as does x_i , and the details of its calculation and those of the zone volumes are given in chapter 3. The time step size, Δt , depends upon several constraints as have been discussed in chapter 4. Not only is it used to control the truncation error in $\frac{\partial \theta}{\partial t}$ and consequently $\frac{\partial \epsilon}{\partial t}$, but it is also used to limit the time for which a calculated flux value must be used. Note from equation (2.21), that depending upon the value for σ , the new and old flux levels are averaged over the time step.

The mean free path at the boundaries is calculated in much the same manner as any other zone. First a boundary interface temperature is found upon which an opacity is calculated. In reference to equation (2.31), this boundary temperature is

$$\phi_0 = \phi_{\frac{1}{2}} \quad \text{if } \beta_0 \neq 0 \quad (5.39)$$

else

$$\phi_0 = \delta_0 \frac{\gamma_0}{\alpha_0} + (1 - \delta_0) \phi_{1/2} \quad \text{if } \beta_0 = 0 \quad (5.40)$$

Then,

$$\kappa_0 = (\theta_0, \rho_{1/2}), \quad \text{and} \quad (5.41)$$

$$\bar{\lambda}_0 = \frac{V_{1/2}}{\kappa_0} \quad (5.42)$$

Similarly at the other boundary,

$$\phi_N = \phi_{N-1/2} \quad \text{if } \beta_N \neq 0, \quad (5.43)$$

$$\phi_N = \delta_N \frac{\gamma_N}{\alpha_N} + (1 - \delta_N) \phi_{N-1/2} \quad \text{if } \beta_N = 0, \quad (5.44)$$

$$\kappa_N = (\theta_N, \rho_{N-1/2}), \quad (5.45)$$

and

$$\bar{\lambda}_N = \frac{V_{N-1/2}}{\kappa_N} \quad (5.46)$$

In the case for which the problem is actually within a pipe, it is necessary to consider the effective reduction in the average mean free path due to the reflection, absorption and re-emission of radiant energy upon the pipe walls. A simple harmonic average of the material and geometric mean free paths is used with a small correction term [7].

$$\frac{1}{\bar{\lambda}} = \frac{1}{\lambda_m} + \frac{1}{\lambda_g} + 0.14 \frac{(\lambda_m/\lambda_g)^{1/2}}{\lambda_m + \lambda_g} \quad (5.47)$$

or

$$\bar{\lambda} = \frac{\lambda_g (1 + \lambda_g / \lambda_m)}{(1 + \lambda_g / \lambda_m)^2 + 0.14 (\lambda_g / \lambda_m)^{1/2}} \quad (5.48)$$

Here, the geometric mean free path

$$\lambda_g = d, \quad (5.49)$$

the diameter of the pipe at the interface in question and λ_m is the so called material mean free path as calculated above in equations (5.36), (5.42) and (5.46).

5.3 Opacity

The opacity tables are of the same form as the equation of state tables. For each tabular density in the form $\ln v_j$, there is a sequence of temperature and opacity pairs, $(\ln \theta, \ln \kappa)_{j,k}$ such that

$$\ln v_1 < \ln v_2 < \dots < \ln v_J, \quad (5.50)$$

$$\ln \theta_{j,1} < \ln \theta_{j,2} < \dots < \ln \theta_{j,K} \quad (5.51)$$

with $J, K > 1$. These tables are also generated by other programs [8], and a great number are available corresponding to the equation of state tables.

The opacity table is interpolated for $\ln \kappa$ from which the mean free path is calculated in equation (5.36). The interpolation formula is simply

$$\ln \kappa(\theta, \rho) = \frac{\ln v - \ln v_j}{\ln v_{j+1} - \ln v_j} (\ln \kappa_{j+1} - \ln \kappa_j) + \ln \kappa_j, \quad (5.52)$$

where

$$\ln \kappa_{j+1} = \frac{\ln \theta - \ln \theta_{j,k}}{\ln \theta_{j,k+1} - \ln \theta_{j,k}} (\ln \kappa_{j,k+1} - \ln \kappa_{j,k}) + \ln \kappa_{j,k} \quad (5.53)$$

$$\ln \kappa_{j+1} = \frac{\ln \theta - \ln \theta_{j+1,\ell}}{\ln \theta_{j+1,\ell+1} - \ln \theta_{j,\ell}} (\ln \kappa_{j+1,\ell+1} - \ln \kappa_{j+1,\ell}) + \ln \kappa_{j+1,\ell} \quad (5.54)$$

assuming that

$$\ln v_j \leq \ln v \leq \ln v_{j+1} \quad \text{with } 1 \leq j < J, \quad (5.55)$$

$$\ln \theta_{j,k} \leq \ln \theta \leq \ln \theta_{j,k+1} \quad \text{with } 1 \leq k < K, \quad (5.56)$$

$$\ln \theta_{j+1,\ell} \leq \ln \theta \leq \ln \theta_{j+1,\ell+1} \quad \text{with } 1 \leq \ell < K. \quad (5.57)$$

As was the case with the equation of state tables, the equations are also used as extrapolation formulae if the density and temperature values are outside of the table limits. This does cause some undesirable problems especially in the low temperature regions.

6.

SOURCE TERMS

In addition to the boundary pressure profiles which have already been discussed, the user may impose time dependent temperature or energy profiles upon any set of zones within the problem. Both may not be done simultaneously, but the user may change from one to the other dynamically as the solution progresses dependent only upon his problem restraints and needs. He may also modify or otherwise change the one he is currently using. Both require time and space dependent profiles. The space dependence is on a zone basis and it is very easily changed. It has been referred to previously as the set of power factors $P_{f_{i+1/2}}$, $i = 0, \dots, N - 1$.

The time dependent temperature or energy profiles are assumed to be in tabular form, but functional forms are simply provided for by the user supplying his own subroutines.

6.1 Energy-Time Profile

An energy table of energy-time pairs in the form (E_j, t_j) may be specified by the user when the program is started, or he may enter or alter the table dynamically during program execution. He need only be careful that

$$t_1 \leq t^n, \quad (6.1)$$

where t^n is the current problem time, and that

$$t_1 \leq t_2 \dots \dots \leq t_j \quad (6.2)$$

with $J \leq 20$. The source energy for each zone is then given by

$$\Delta S_{1+1/2}^{n+1/2} = P_{f_{1+1/2}} \frac{(E_{j+1} - E_j)}{(t_{j+1} - t_j)} \Delta t^{n+1/2}, \quad (6.3)$$

where

$$t_j \leq t^n < t^{n+1} \leq t_{j+1}. \quad (6.4)$$

If the time step size is so large as to extend over parts of more than one table interval, then the source integration is done piece-wise in order that the problem will reflect the correct total energy at all times. If

$$t_j < t^n, t^{n+1} \quad (6.5)$$

then the table is simply extrapolated in a linear fashion using the last two entries. This of course implies that the table must have a minimum of two entries. Note that the table need not even be piece-wise continuous and that multiple entries may be given for the same time. This facilitates step as well as ramp energy excursions. For example, if

$$t_{j-1} \leq t^n < t_j = t_{j+1} < t^{n+1} \leq t_{j+2}, \quad (6.6)$$

then

$$\Delta S_{1+1/2}^{n+1/2} = P_{f_{1+1/2}} \left[\frac{E_j - E_{j-1}}{t_j - t_{j-1}} (t_j - t^n) + (E_{j+1} - E_j) + \frac{E_{j+2} - E_{j+1}}{t_{j+2} - t_{j+1}} (t^{n+1} - t_{j+1}) \right]. \quad (6.7)$$

Care should be taken to insure that $t_{j-1} \neq t_j$.

6.2 Temperature-Time Profile

The structure of a temperature profile is not unlike that which has been given for an energy profile. It is a profile of temperature time pairs of the form (θ_j, t_j) specified in the same manner as is the energy profile. The purpose of this profile is to impose a temperature over a set of zones within the problem. These zones thus act much like a time dependent heat reservoir, be it a sink or a source. The imposition of the profile over a specific set of zones is done through the power factors. If $P_{f_{i+k}} = 1$, then this is used as a flag to indicate that the temperature of this zone is determined by the profile. Likewise, if $P_{f_{i+k}} = 0$, then the temperature of this zone is not dependent directly upon the profile.

Rather than simply "overloading" the specified zones with the temperature as given by the profile, it is desirable to calculate the source term necessary to give this temperature for each zone in question. It is then possible for the user to monitor the amount of energy being "dumped" into (or out of) the problem. He is also able to monitor the overall problem energy balance.

The first step toward calculating this source term is to interpolate the profile for the current temperature:

$$\theta = \frac{\theta_{j+1} - \theta_j}{t_{j+1} - t_j} (t^{n+1} - t_j) + \theta_j, \quad (6.8)$$

where

$$t_j \leq t^{n+1} \leq t_{j+1}. \quad (6.9)$$

Then, the extrapolation procedure depicted in figure 3 and given by equation (2.53) is modified as follows:

$$\theta_{i+1/2}^{n+1/2} = \begin{cases} v \frac{\Delta t^{n+1/2}}{\Delta t^{n-1/2}} (\theta_{i+1/2}^n - \theta_{i+1/2}^{n-1}) + \theta_{i+1/2}^n & \text{if } P_{f,i+1/2} = 0, \\ \hat{\theta} & \text{if } P_{f,i+1/2} \neq 0. \end{cases} \quad (6.10)$$

After obtaining an estimate of the zone temperatures as indicated above, the temperature dependent terms are updated as indicated by equations (2.54), (2.55), (2.56), (2.57), (2.58) and (2.59). The source term $k_{\Delta S_{i+1/2}}^{n+1/2}$ is then calculated (and recalculated for each iteration) through equations (2.36), (2.37) and (2.38) by replacing each $k_{\phi_{i+1/2}}^{n+1}$ by $\hat{\phi} = \hat{\theta}^4$ if $P_{f,i+1/2} \neq 0$. Note also, that source terms are calculated only for those zones for which $P_{f,i+1/2} \neq 0$. In actual practice, $P_{f,i+1/2}$ is used as a multiplicative factor when solving for $k_{\Delta S_{i+1/2}}^{n+1/2}$ from each equation.

If $t^{n+1} > t_j$, then equation (6.8) is used as an extrapolation formula.

7.

COMPUTER CALCULATIONS

A number of calculations were done to illustrate the effect and the worth of various program parameters and to also validate the method of solution. In addition, F^3 , a one-dimensional program at Los Alamos [5], was used to do some of the same calculations. A three way comparison was then made with the analytical solutions.

The program developed from the method given in this paper is referred to as HYRAD1. It has been programmed to run on the PDP-10 computer at the University of Utah via the remote terminal at Montana State University and also on both the CDC-6600 and CDC-7600 computers at Los Alamos. The 6600 and 7600 versions are identical, being FORTRAN programs, but are restricted at this time to plane geometry problems only.

7.1 Radiation Diffusion Calculations

A series of calculations is presented here which was used to validate the radiation diffusion calculations and to illustrate the effect and worth of several program parameters. A complete description of the problem, often referred to as the Marshak Wave Problem, may be found in [9]. The basic elements are as follows:

1. Constant specific heat, $\frac{\partial \epsilon}{\partial \theta}$.
2. No energy in the radiation field.
3. Constant density, ρ .
4. An opacity $\kappa = \kappa_0 \rho^a \theta^{-B}$.
5. Constant driving temperature, θ_0 .
6. Plane geometry.

Thus, for simplicity:

$$\frac{\partial \epsilon}{\partial \theta} = \frac{ac}{3} \frac{2}{\kappa_0} \frac{4}{n+4}$$

$$\rho = 1$$

$$\kappa_0 = 1.0$$

$$a = 1$$

$$\theta_0 = 1$$

$$\theta_{1+1/2}^0 = 10^{-6} \sim 0$$

(7.1)

In addition, a unit cross sectional area was assumed. Several values for β were tried in addition to varying length zones, etc. Corresponding to the tables published in [9], the space and temperature values were normalized as follows:

$$\xi_{1+1/2}^n = \frac{x_{1+1/2}^n}{\sqrt{t}^n} \quad (7.2)$$

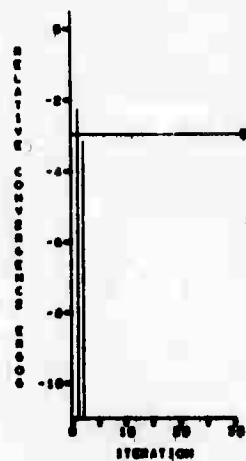
$$\tau_{1+1/2}^n = \theta_{1+1/2}^n / \theta_0 = \theta_{1+1/2}^n \quad (7.3)$$

The calculations could then be checked at any time for which there was a $x_{1+1/2}$ which gave rise to a $\xi_{1+1/2}$ that appeared in the published tables. This was not difficult since tabular values were given in increments of 0.05 for ξ starting with $\xi = 0$ and $\tau = \theta_0 / \theta_0 = 1$ out to where $\tau = 0$. No interpolation was necessary nor desired.

The purpose of these calculations is to follow the diffusion of a radiation wave driven by a constant boundary temperature. Its progress is then checked at various times with respect to its position and shape. Figures 4 through 10 give the position of the wave at

different times as a temperature profile. In these display console pictures, the temperature, pressure and density increase to the right, and the x coordinate increases in the vertical direction. The density curve at the right is constant over all time and the horizontal lines are indicative of the zone boundaries.

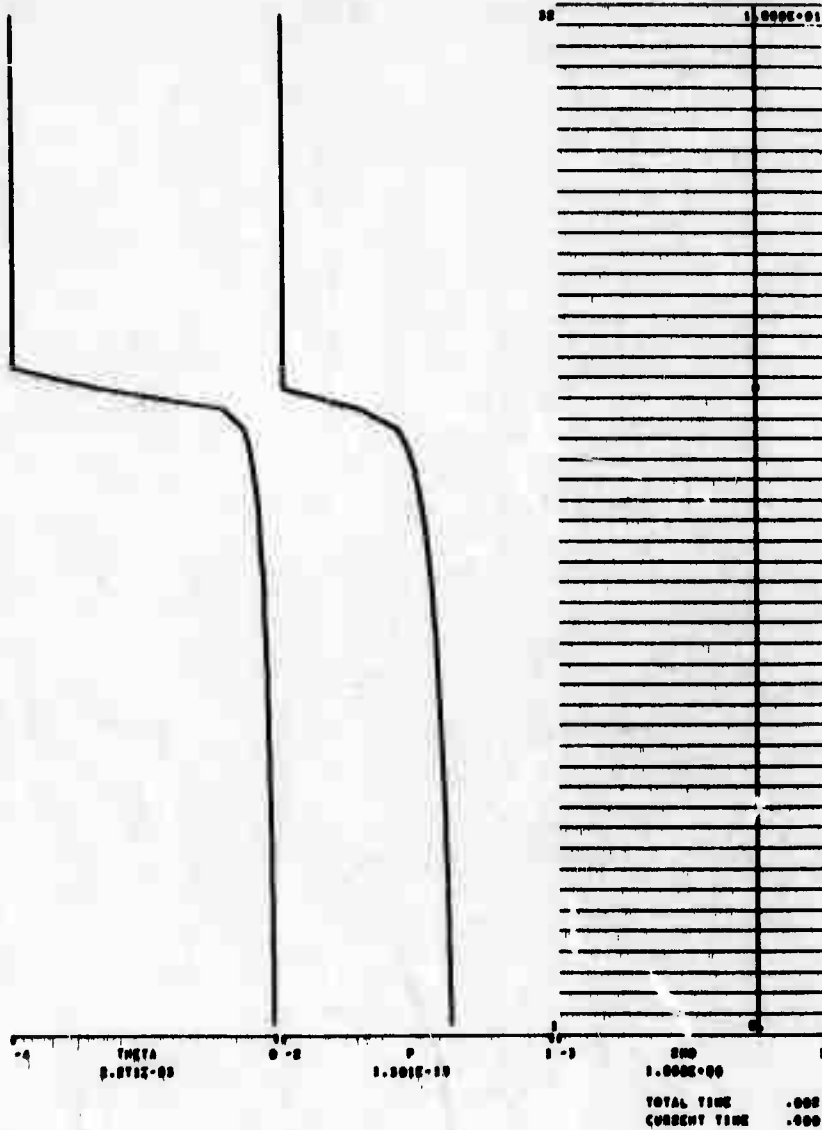
1 2.100000E+01
 07 1.70000E+02 P
 NTS 1001



CH00A111 .000
 CH00A101 .000
 CH00A101 .000
 CH00A101 .000
 TVAC .1000 QTY 0.10E+02 02
 WFAC .0100 WTH 1.00E+10 1
 CFAC .0000 QTC 0.01E+00 1
 MU 1.000 SIGMA 1.000
 IS 1.001E+00
 IS 0.
 IS 1.001E+00
 IS 1.001E+00

HARDMAX-10

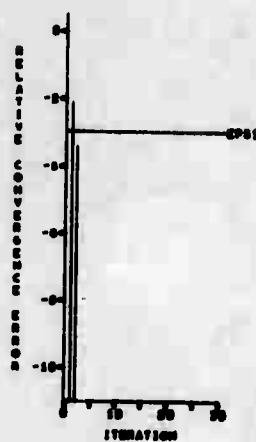
ZONE MATERIAL
 SE WING



TOTAL TIME .000
 CURRENT TIME .000

Figure 8

Y 4.00000E+01
 OT 1.14700E+00 P
 HTS 0000



OMEGA(1) .000
 OMEGA(2) .000
 OMEGA(3) .000
 OMEGA(4) .000
 TFAC .1000 OTT A.07E+00 A0
 HFAC .0100 OTH 1.00E+10 1
 CFAC .0000 OTC 0.01E+02 1
 MW 1.000 110MA 1.000
 IE 1.007E+00
 IE 0,
 1.007E+00
 DE 1.007E+00

HARDMAN-10

SOME MATERIAL
 AS NINE

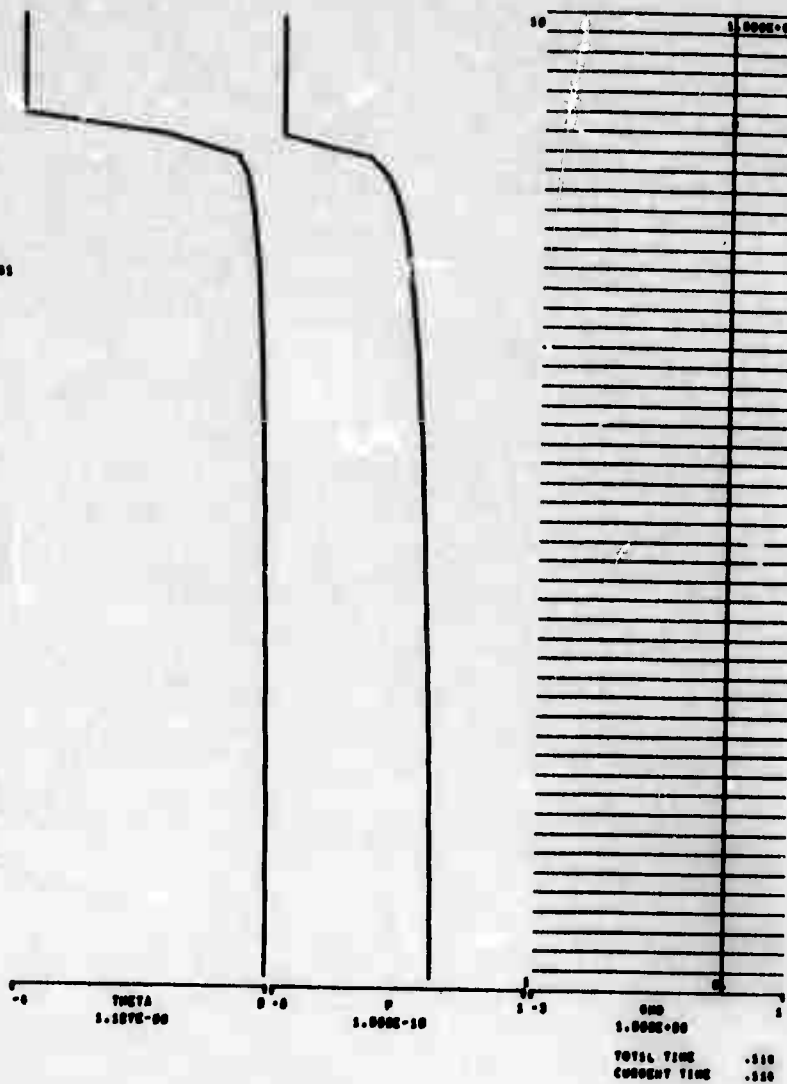


Figure 10

Note that a constant density prohibits any hydrodynamic activity and that this problem is purely a radiation diffusion calculation. The first series of problems was done with $\beta = 0$ and the zone width $\Delta x_{i+1} = .2$ cm. Thus, $\lambda = \frac{1}{\kappa_0} = .1$ cm, only half the zone width. The initial temperature distribution, $\theta_{i+1/2}^0 = 10^{-6}$, is sufficiently close to zero and is very near the calculational limit of the PDP-10 for $\phi = \theta^4 = 10^{-24}$ and $\frac{\partial \epsilon}{\partial \theta} = 0.2 \frac{ac}{3} = 0.274442$.

Table 1 below gives the exact solution and corresponding values for τ as calculated by HYRAD1 and F^3 at common values of ξ for $t = 36$ sh. The tabular entries are rounded to five digits, and it is important to point out that even in double precision, some significance in the fifth digit is the most one can expect on the PDP-10 computer. For HYRAD1, $\sigma = 1/2$, $v = 1$, $\epsilon = 10^{-5}$, $T_{\text{fac}} = .10$, and $\Delta t^0 = 10^{-7}$ sh. While for F^3 , $T_{\text{fac}} = .10$ and $\Delta t^0 = 10^{-8}$ sh.

ξ	τ	HYRAD1	F^3
.05	.98803	.98803	.98803
.15	.96273	.96272	.96272
.25	.93538	.93537	.93537
.35	.90563	.90562	.90562
.45	.87304	.87303	.87303
.55	.83699	.83697	.83697
.65	.79661	.79658	.79658
.75	.75061	.75056	.75056
.85	.69692	.69685	.69685
.95	.63187	.63177	.63177
1.05	.54763	.54754	.54755
1.15	.42047	.42008	.42009
1.25	0	.00638	.00637
S.E.(j)	1.5490	1.5489	1.5504
I.E.(j)	1.5490	1.5489	1.5489
# time steps		2316	2327
avg. # iterations		6.1	1
calculation time (min)			
@ 49 sh	7600	1	.4
	PDP-10	64	

Table 1: HYRAD1 and F^3 Calculations As Compared With The Analytical Solution For $\kappa = 10$.

The next three sets of tables and figures illustrate the difference caused by variations in σ , ν , T_{fac} and ϵ as calculated by HYRAD1. In table 2 and figure 11 the only changes in τ occur between $\sigma = \frac{1}{2}$ and $\sigma = 1$ for $\epsilon = 10^{-5}$ and $T_{fac} = .10$. For $\sigma = 0$, the calculations go unstable after 6 shakes when $\Delta t > 1.5 \times 10^{-2}$. The results at 4 shakes are impressive though, being much better than those for $\sigma = \frac{1}{2}$. The severe time step size restriction for this parameter value is less than desirable and no further calculations were tried at this time with $\sigma = 0$. The effect of the extrapolation parameter ν is to reduce the number of iterations required for each time step advancement. For this and most problems it is most effective at unity. For some problems, adjusting ν can reduce the number of iterations by as much as a third.

Running times as given for the PDP-10 are approximate and vary several minutes depending upon the machine activity (i.e. the number of times the program must be swapped).

σ	v	Number of Time Steps	Avg. Number of Iterations	PDP-10 Computer Time (Min)
0	1		(unstable)	
.5	1	2316	6.1	64
1	1	2304	6.1	64
1	.5	2304	7.1	74
1	0	2304	7.3	75

Table 2: Variations in the Time Differencing and Extrapolating Parameters, σ and v , at $t = 49$ sh.

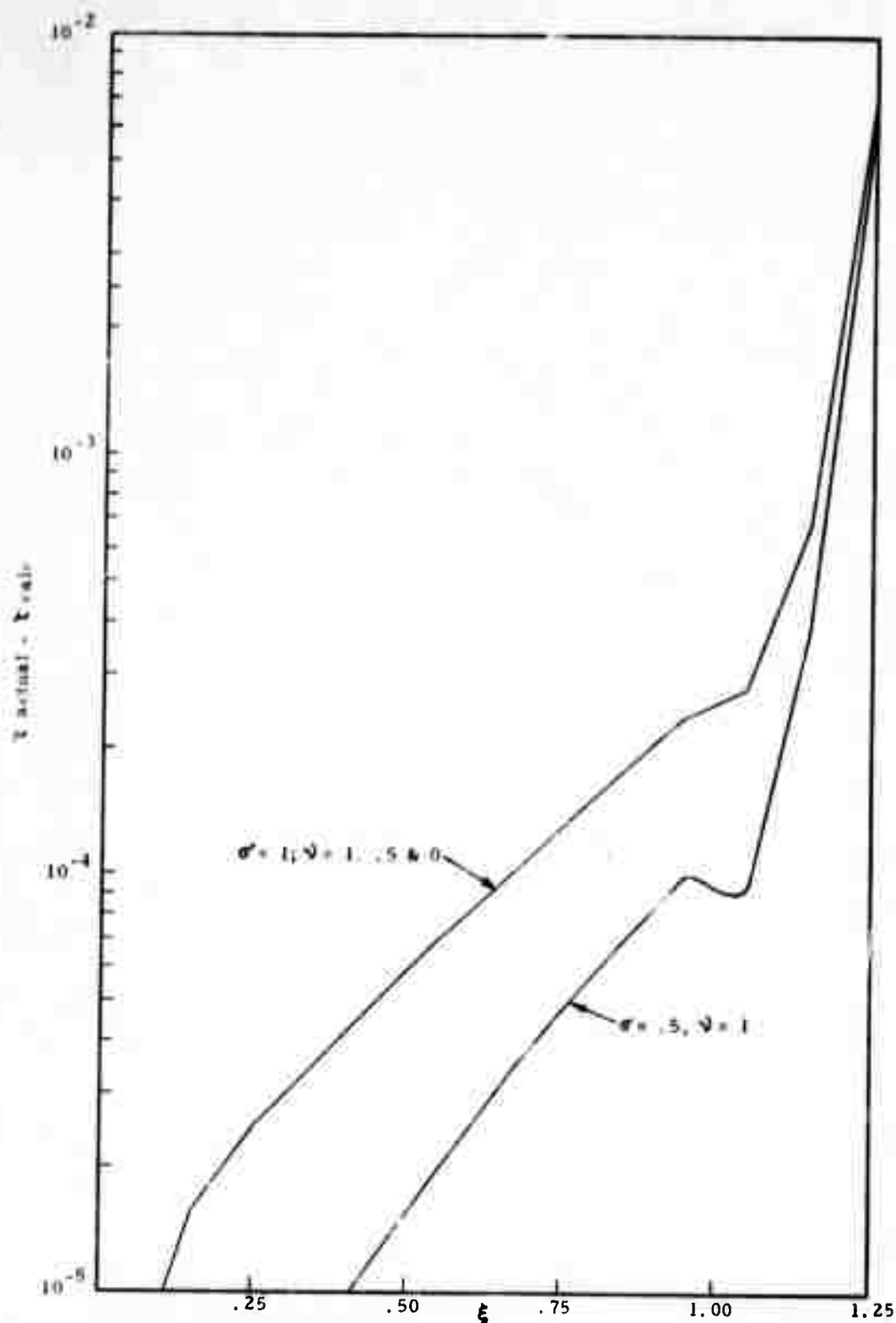


Fig. 11: Variations in the time differencing and extrapolating parameters σ and ν at 36 sh.

Table 3 and figure 12 show the relative insensitivity of results upon the time step size restriction factor T_{fac} for $\sigma = 1$, $\nu = 1$ and $\epsilon = 10^{-5}$. This also holds true for $\sigma = 1/2$. Note, however, that it does dramatically affect the calculation time directly by limiting the time step size.

T_{fac}	Number of Time Steps	Avg. Number of Iterations	Avg. Δt (sh)	PDP-10 Computer Time (Min)
.01	27993	2.2	.00175	295
.05	5478	4.2	.00895	100
.10	2661	6.1	.01841	70
.15	1720	7.8	.02849	52
.20	1248	9.6	.03926	46
.25	966	11.4	.05072	42
.30	774	13.2	.06331	41
.35	641	15.1	.07644	38
.40	540	16.9	.09074	36

Table 3: Variations in the Temperature Restriction Factor, T_{fac} , at $t = 49$ sh.

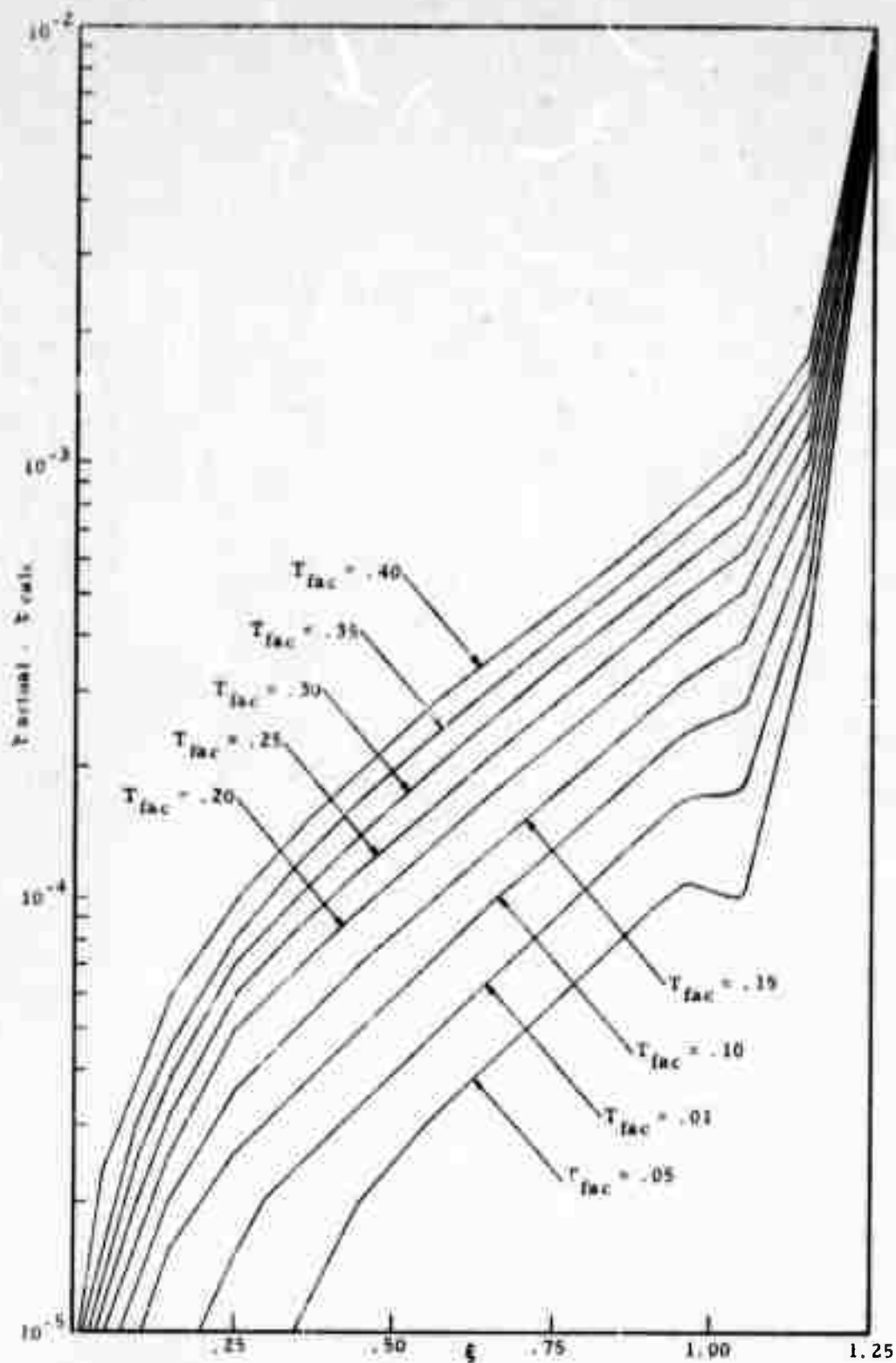


Fig. 12: Variations in the temperature change restriction factor, T_{fac} , at 36 sh.

Table 4 and figure 13 illustrates the significance of the convergence parameter with $\sigma = 1$, $\nu = 1$ and $T_{fac} = 0.1$. For values of ϵ less than or equal to 10^{-4} , the results are unaffected. This is expected since 4-5 digits of significance is all that can be obtained on the PDP-10. What is impressive is the reasonably good results for $\epsilon = 10^{-1}$. Take note also of the variance in the average number of iterations per time step and its effect upon the calculational time.

ϵ	I.E. (j)	S.E. (j)	Number of Time Steps	Average Number of Iterations	PDP-10 Computer Time (Min)
10^{-7}	1.806998	1.806998	2662	8.8	90
10^{-6}	1.806998	1.806998	2662	7.4	80
10^{-5}	1.806998	1.806999	2661	6.1	70
10^{-4}	1.806997	1.806999	2661	4.8	58
10^{-3}	1.806966	1.807028	2661	3.2	39
10^{-2}	1.806708	1.807243	2662	1.8	28
10^{-1}	1.806070	1.807762	2671	1.0	23
actual	1.807152	1.807152			

Table 4: Variations in the Convergence Parameter, ϵ , at $t = 49$ sh.

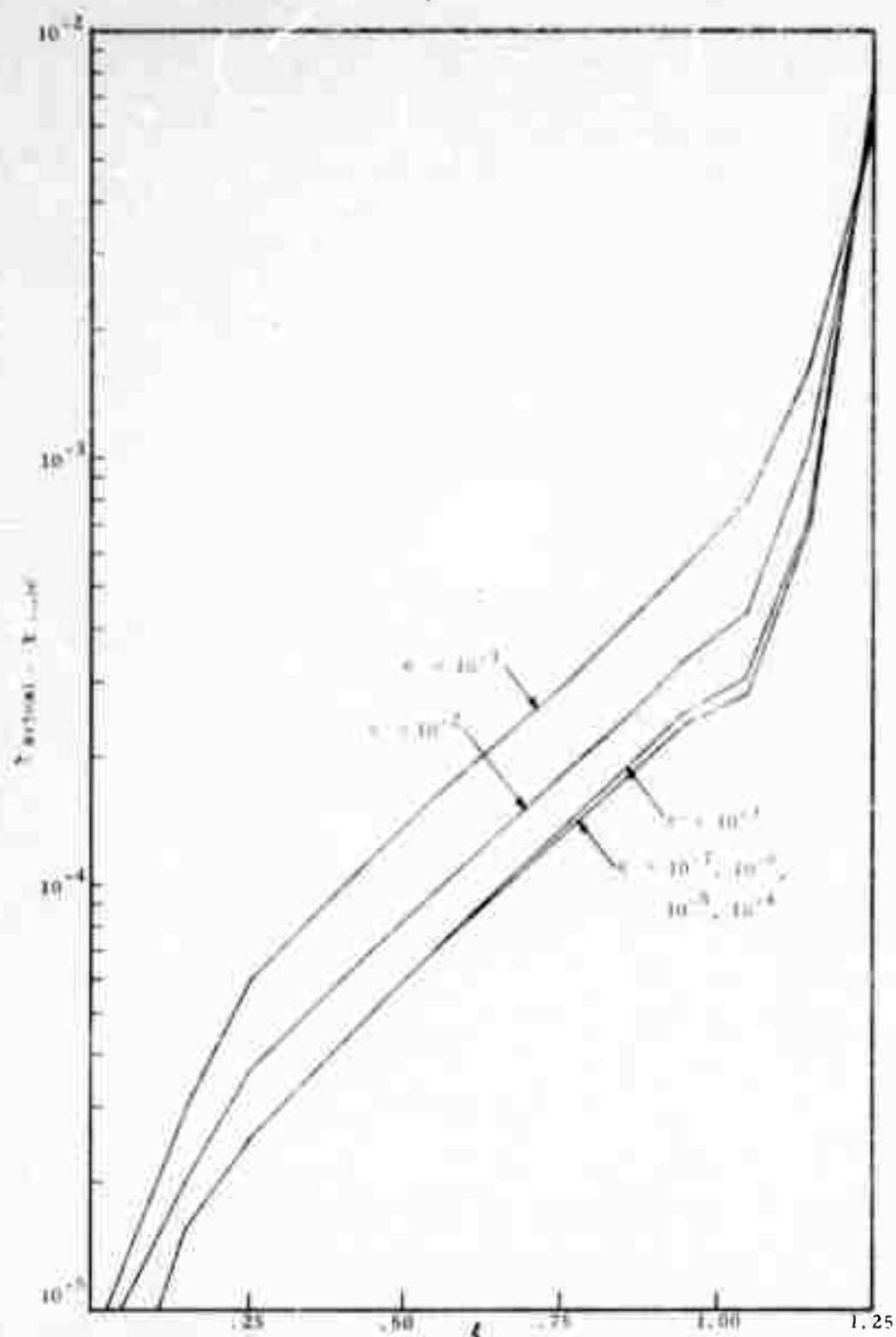


Fig. 13: Variations in the convergence parameter, ϵ , at $t = sh$.

Several other calculations were done with other values of β .

Table 5 gives the results for a calculation at 36 sh. done with $\beta = 3$.

For this case, $C_v = \frac{4}{35} \frac{ac}{\beta} = .156825$, $\lambda = \frac{\theta^3}{10}$, $\sigma = 4$, $\nu = 1$, $\epsilon = 10^{-5}$, $T_{fac} = .10$ and $\Delta t^0 = 10^{-7}$ sh., and for F^3 , $T_{fac} = .10$ and $\Delta t^0 = 10^{-8}$ sh.

ϵ	τ	HYRAD1	F^3
.05	.94296	.99297	.99297
.15	.97792	.97793	.97793
.25	.96139	.96141	.96141
.35	.94304	.94307	.94307
.45	.92242	.92246	.92246
.55	.89887	.89891	.89892
.65	.87136	.87141	.87142
.75	.83820	.83828	.83828
.85	.79616	.79635	.79634
.91	.73785	.73849	.73845
1.05	.63704	.63945	.63933
1.15	0	.00021	.00015
S.E.(j)	.90914	.90917	.90989
I.E.(j)	.90914	.90917	.90887
# time steps		2457	2468
avg. # iterations		5.9	1
calculation time			
@ 49 sh.	CDC-7600	1 min	.4 min
	PDP-10	68 min	

Table 5: HYRAD1 and F^3 Calculations as Compared with the Analytical Solution for $\kappa = 10/\theta^3$.

Another series of problems were run for a variety of zone widths from 0.1 cm to 200 cm. The difference in the results were significant and improved with smaller Δx 's approaching the mean free path. This just confirms one's intuition that the linear space derivative approximation for $\frac{\partial \phi}{\partial x}$ does not adequately describe the flux terms for coarse zoning even for materials which exhibit constant or nearly constant opacities. So much concern and work has been directed toward calculating

a mean free path at the interface between zones, whereas it should probably be directed at arriving at a better flux term as a whole. Of course, this is difficult to do properly, for there is just not enough information. In most cases, it is usually better to zone finer. No calculations were done with zone widths less than a mean free path.

One interesting result obtained from the variable zone width calculations was the invariance of the results on a time step by time step basis. More precisely, if the calculation time is normalized with respect to the square of the multiplicative difference in zone widths, then the results at comparable normalized times are the same. For example, the temperature profile at $t = 9$ sh for $\Delta x = 0.1$ is the same as for $t = 36$ sh for $\Delta x = 0.2$, but the latter calculation includes exactly twice as much energy.

7.2 Hydrodynamic Calculations

In this section, a series of hydrodynamic calculations are presented. Two different problems were investigated. The first is a shock-tube problem which is described in [10] and [11]. This calculation follows the shock formed by a high pressure gas expanding into a low pressure gas confined in a long small radius pipe or tube. The problem assumes an ideal gas for which

$$c = p/\rho(\lambda-1) \quad (7.4)$$

$$p = \rho R\theta, \quad (7.5)$$

with

$$\lambda = C_p/C_v. \quad (7.6)$$

$$R = C_p - C_v. \quad (7.7)$$

For air, $\lambda = 1.4$ and $R = 286.793 \text{ m}^2/\text{sec}^2 \text{ } ^\circ\text{K}$ assuming 29 grams/mole of air.

From equations (7.4) and (7.5),

$$\begin{aligned} \frac{\partial \epsilon}{\partial \theta} &= C_v, \\ &= R/\lambda - 1, \\ &= \frac{5}{2} R, \\ &= 716.983 \text{ m}^2/\text{sec}^2 \text{ } ^\circ\text{K}, \end{aligned} \quad (7.8)$$

$$\frac{\partial \epsilon}{\partial v} = 0. \quad (7.9)$$

For the one region of gas, $p = 666.447 \text{ kg/m-sec}^2$ and $\rho = .0077459716 \text{ kg/m}^3$, and for the other region $p = 1.1823 \times 10^7 \text{ kg/m-sec}^2$ and $\rho = 137.413 \text{ kg/m}^3$. The initial temperature for both regions is 300°K .

The first calculation done was with a constant $\Delta x = .0254 \text{ m}$, $\Delta t = 1.25 \times 10^{-6} \text{ sec}$, $r = .0254 \text{ m}$ and an artificial viscosity factor $\eta_1 = 0.8$. The results of this calculation match the results for the KO and PUFL programs as reported in [10]. The next calculation was done with $\eta_2 = 2$. Again the overall result was the same. However, when the region at and behind the shock front was examined in detail, the quadratic form of artificial viscous pressure exhibited rather large oscillations as displayed in the pressure profile given in figure 14. Notice in contrast the smooth pressure profile for the linear form of the viscous pressure term. A combination was then tried with $\eta_1 = 1$ and $\eta_2 = 3$ as suggested in [10]. These results were identical with the linear case except right at the shock front which is not as sharp and is extended over several more zones.

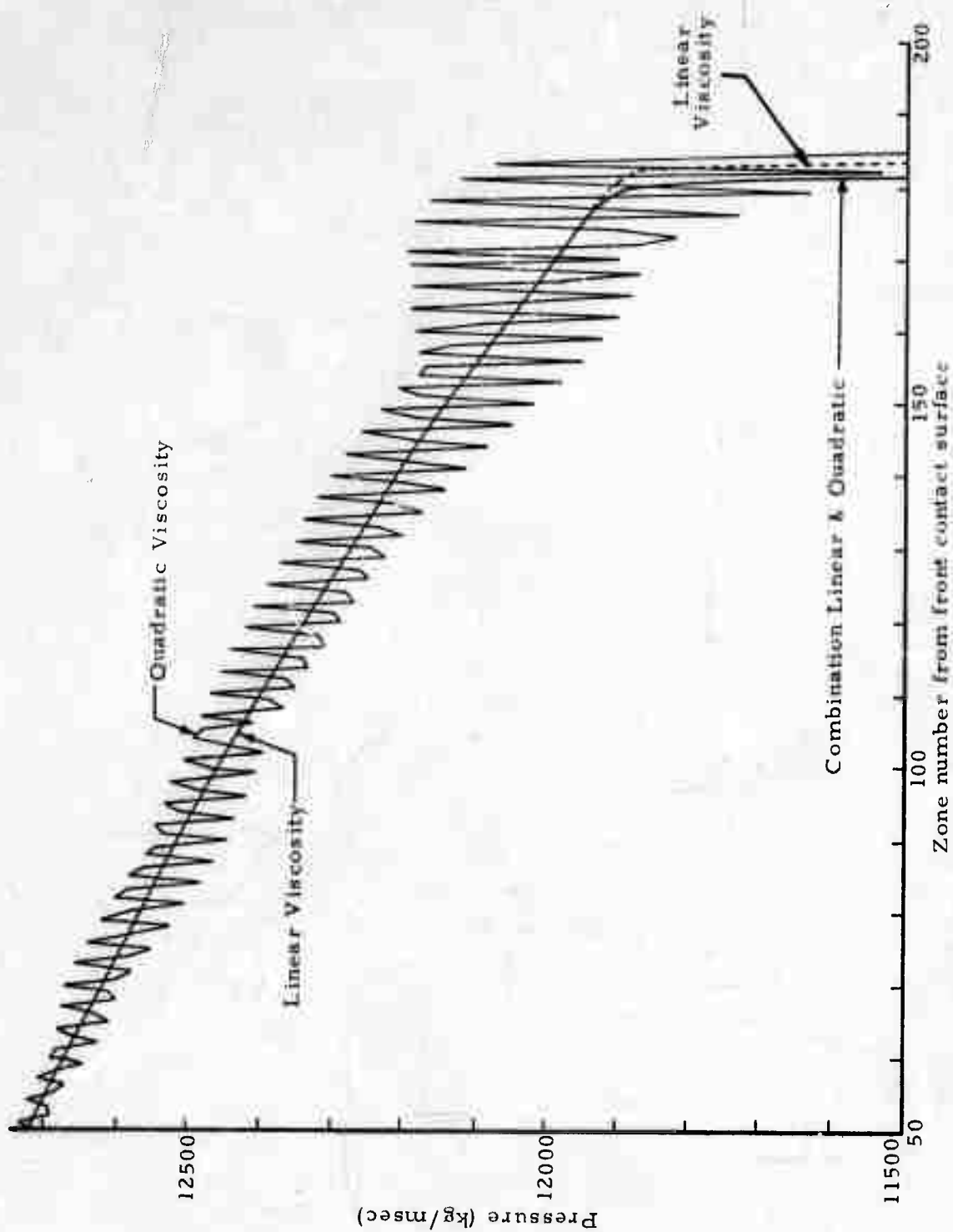


Fig. 14: Pressure profile in region 2 for different viscosity terms at $t = .0080$ sec.

Another series of calculations were done with a variable Δt . For this series, the major time step restriction from those discussed in chapter 4 is the hydrodynamic restriction determined by the parameter H_{fac} . Two calculations were done with $H_{fac} = .05$ and $.10$ and there was little significant difference in the results as shown in figure 15. However, there was a great difference in the calculational efficiency as indicated by table 6.

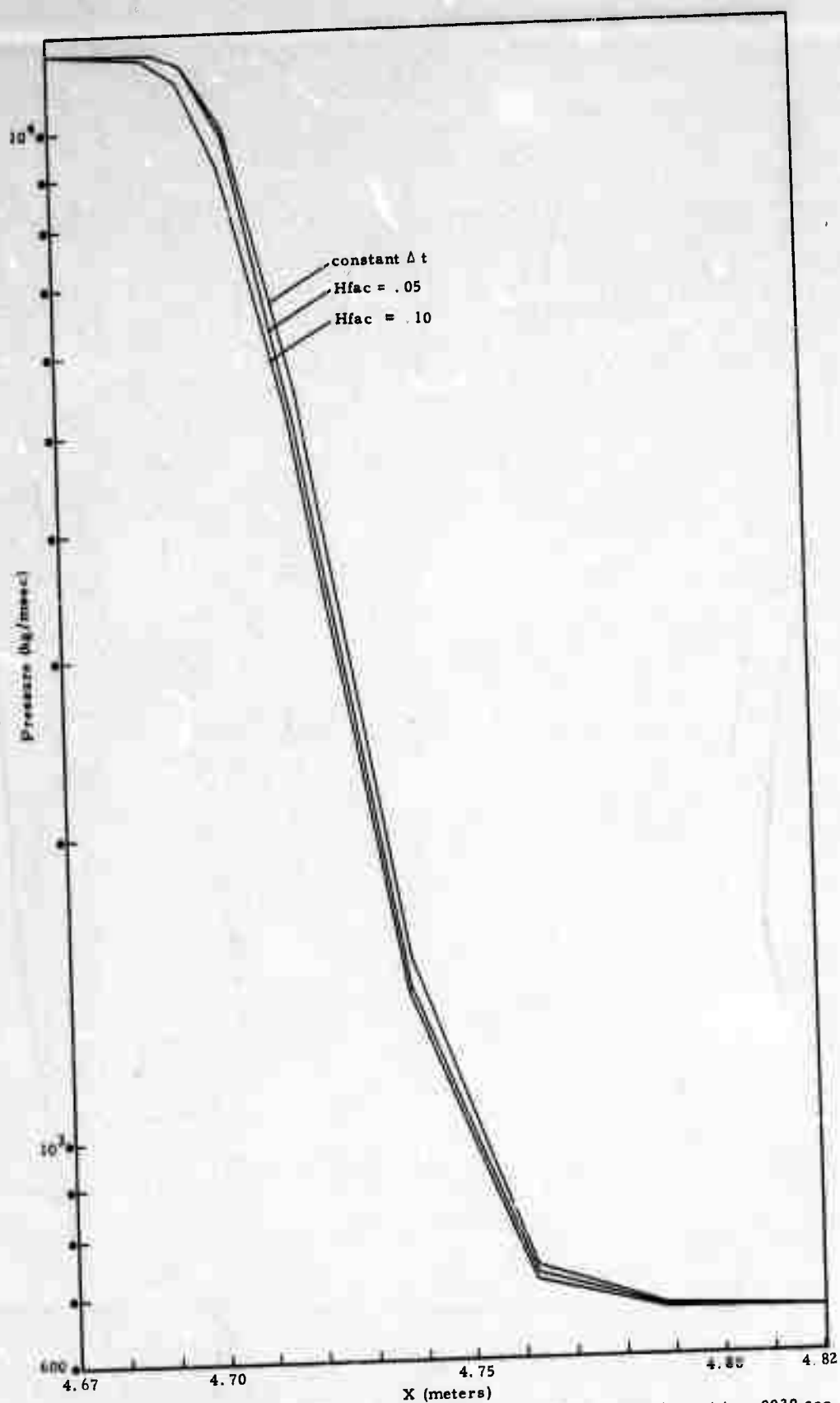


Fig. 15: Pressure profile at shock front for different time step restrictions at $t = .0039$ sec.

	Constant Δt	$H_{fac} = .05$	$H_{fac} = .10$
avg. time step size (sec)	1.25×10^{-6}	1.915×10^{-6}	4.004×10^{-6}
total number of time steps	3120	2037	974
avg. number of iterations per time step	4.7	5.7	7.5
PDP-10 calculational time (min)	228	151	92
K.E. (j)	2.02030×10^4	2.01989×10^4	2.02013×10^4
I.E. (j)	-2.02063×10^4	-2.02033×10^4	-2.02037×10^4

Table 6: Relative Calculational Efficiency of Constant vs. Dynamic Time Step Sizes at $t = .0039$ sec.

Another calculation done was with a constant Δt but with $\Delta x = .0508$ meters, double that of the previous calculations. As was the case with the pure radiation diffusion calculations, the solution was very sensitive to the zone width. Figure 16 gives the difference in the pressure profiles at the time, $t = .0039$ sec.

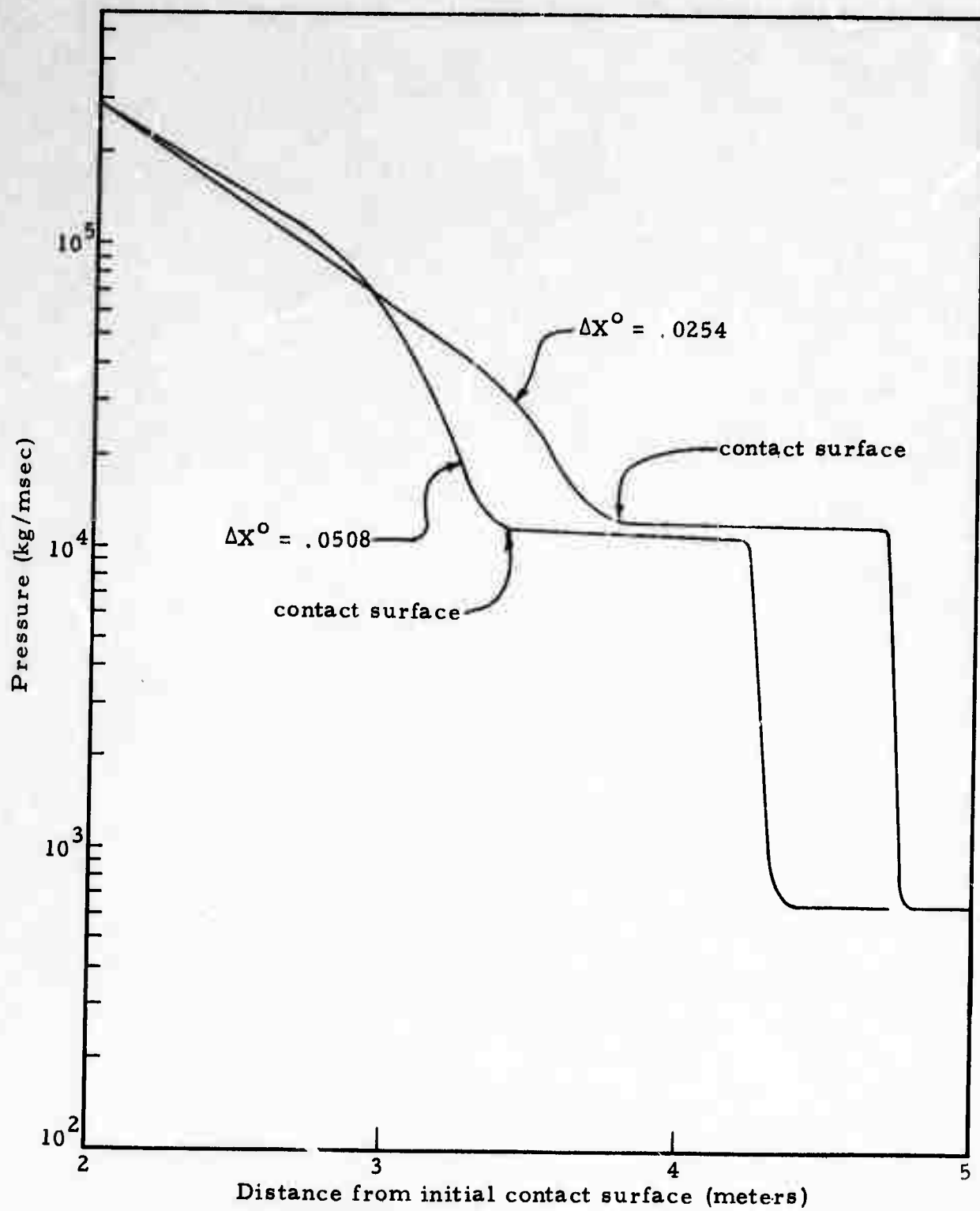


Fig. 16: Pressure profile for different zone widths at $t = .0039$ sec.

The final set of calculations done in the shock tube series was with a non-uniform radius tube. Here, a conic section, or frustrum was initially specified as the container of the low pressure gas. The high pressure gas was then allowed to expand into this volume as before. In this conic section, the radius increased linearly at the rate of one inch to every ten along the axis from an initial one inch radius. The calculations started with initial one inch (.0254 m) zone widths and specified a constant $\Delta t = 1.25 \times 10^{-6}$ sec.

The first problem was run in the normal fashion with the zone center placed at the center of volume (as approximately given in section 3.1). The second problem was identical except that the zone center was placed at the mid-point between the zone interfaces as shown in figure 17. The latter is referred to as the axial mid-point or zone center.

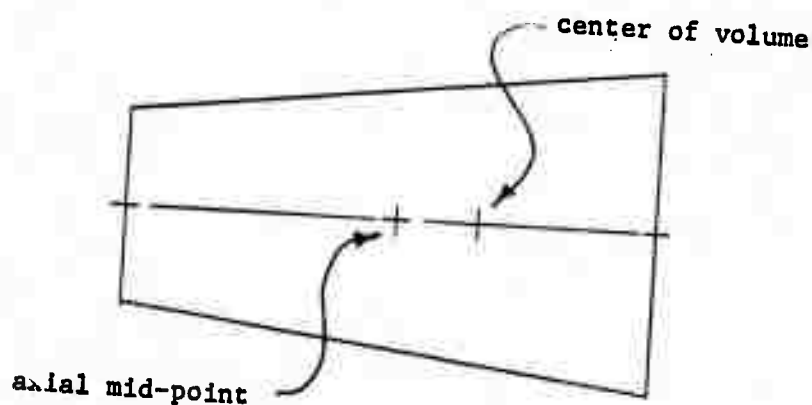


Fig. 17: Zone Mid-Point Definitions

The results of the calculations are given in figure 18 at $t = .0005$ and $.001$ seconds in the form of temperature profiles. The temperature was used here in lieu of the pressure because it did not vary over as wide a range of values, but is directly proportional and indicative of the pressure. In both cases, figure 18 shows that the peak temperatures in the center of volume problem are greater and are advanced further down the tube than those for the axial center problem.

Table 7 gives the program statistics for this set of calculations. Note that for this geometrical configuration, the kinetic energy as given by equation (2.64) does not match the loss in internal energy. This was not the case for the constant diameter problems as shown in table 6. At about $.00075$ sec, the problem became Courant limited (see section 4.1) because the shock was encountering larger and more massive zones as the pipe diameter increased. Thus, the zones tended to pile up into smaller widths.

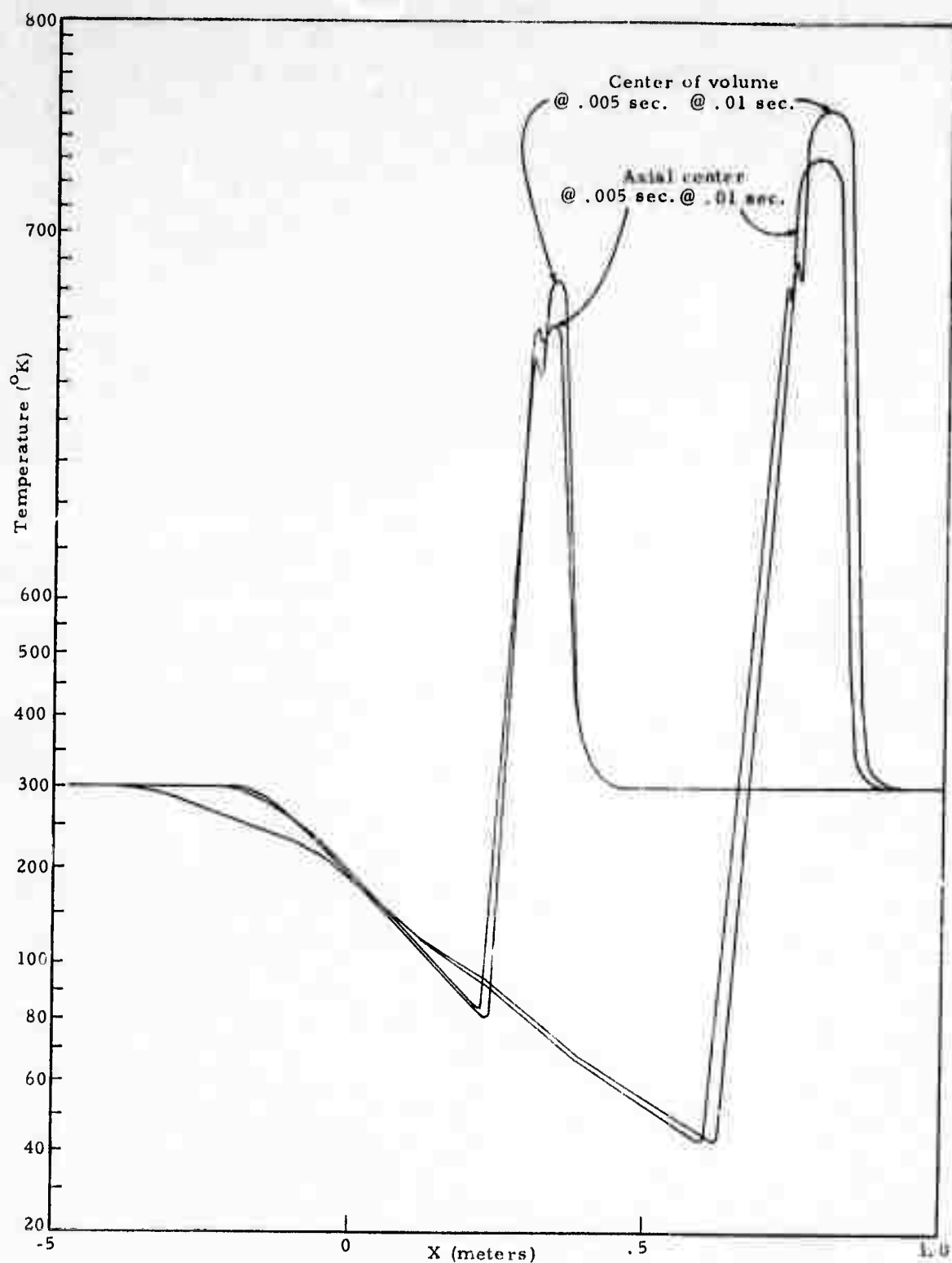


Fig. 18: Temperature profile of volume vs. axial zone center at .005 and .01 sec.

84

	Axial Center	Volume Center
time step size (sec.)		
@ .0005 sec.	1.25×10^{-6}	1.25×10^{-6}
@ .001 sec.	6.48×10^{-7}	6.11×10^{-7}
total number of time steps		
@ .0005 sec.	401	401
@ .001 sec.	908	933
avg. number of iterations		
@ .0005 sec.	2.7	2.7
@ .001 sec.	2.9	2.9
PDP-10 calculational time (min)		
@ .0005 sec.	9.9	10
@ .001 sec.	23.3	23.6
K.E.		
@ .0005 sec.	3.23157×10^3	3.19644×10^3
@ .001 sec.	7.22040×10^3	7.11488×10^3
I.E.		
@ .0005 sec.	-3.14898×10^3	-3.11402×10^3
@ .001 sec.	-6.82762×10^3	-6.76969×10^3

Table 7: Program Statistics for Axial vs. Volume Zone Centers

The second problem investigated in the hydrodynamic series is known as the Von Neumann point source problem [12]. The purpose of this problem, also known as the blast problem, is to calculate as a function of time the blast radius propagating from the blast point in spherical geometry. The Von Neumann solution to the blast problem is given in [12] and numerical solutions are given in [13] and [14]. This problem is similar to the shock tube problem in that it assumes an ideal gas equation of state (equations 7.4 through 7.9), but differs in that a large amount of energy is released at (near) the center of a spherical volume.

Eilers and Whitfill at Los Alamos have been using this problem to validate numerical integration techniques and to establish parametric values. In particular, they provided several calculations done with

the F^3 program for comparison with HYRAD1 and the analytical solution given by [12]. One such solution is given in figure 19 together with that from HYRAD1 and variations therein. Figure 19 is a plot of the absolute difference between the actual blast radius and the calculated blast radius as a function of time. For this series, $\Delta x_1^0 = 30.5$ cm, $\gamma = 1.2$, $\frac{\partial \epsilon}{\partial \theta} = 5$, $\frac{\partial \epsilon}{\partial v} = 0$, $R = 1$ (meaning θ absorbs the actual value of R), $\theta_{i+\frac{1}{2}}^0 = 10^{-6}$, $\eta_1 = .8$, $T_{fac} = .10$, $\theta_p = .001$, $H_{fac} = .01$, $\Delta t^0 = 10^{-7}$ and (the energy-in at the blast point) $E_{in} = 4185_j$.

At this point, it is important to point out the difference in the acceleration terms as calculated in F^3 [5] with those calculated by HYRAD1. F^3 uses the following difference equation to arrive at a numerical solution to the momentum equation:

$$\ddot{x}_1 = \frac{4\pi x_1^2}{\frac{1}{2}(m_{1-\frac{1}{2}} + m_{1+\frac{1}{2}})} (p_{1-\frac{1}{2}} - p_{1+\frac{1}{2}}) \quad (7.10)$$

which is equivalent to

$$\ddot{x}_1 = \frac{v_1}{\frac{1}{2}(m_{1-\frac{1}{2}} + m_{1+\frac{1}{2}})} \frac{(p_{1-\frac{1}{2}} - p_{1+\frac{1}{2}})}{\Delta x_1} \quad (7.11)$$

where

$$\Delta x_1 = x_{1+\frac{1}{2}} - x_{1-\frac{1}{2}}$$

$$x_{1+\frac{1}{2}} = \frac{1}{2}(x_1 + x_{i+1}) \quad (7.12)$$

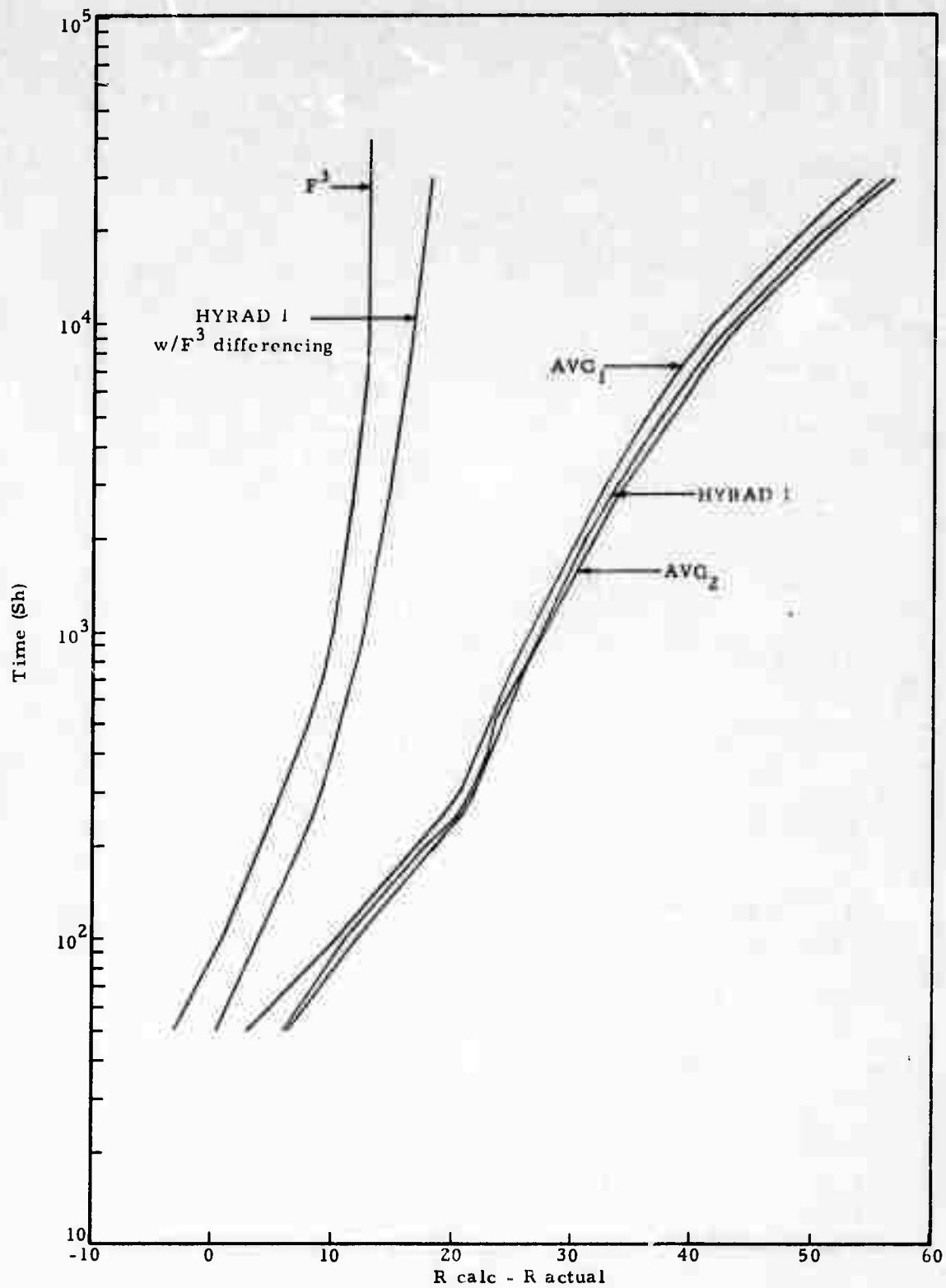


Fig. 19: Comparison of hydrodynamic differencing schemes.

Equation (7.11) is now in the same form as given for HYRAD1 in equation (2.7). The quantity $x_{i+\frac{1}{2}}$ as given in (7.12) is said to be located at the radial center in contrast to the center of volume as specified for HYRAD1 by equation (3.28). The difficulty with equation (7.11) is the location of the volume given by V_i . The denominator term implies that it should include half the mass of each adjacent zone if a uniform density is assumed as is done in HYRAD1. In contrast then,

$$V_i = 4\pi x_i^2 \Delta x_i, \quad (7.13)$$

which when expanded becomes:

$$V_i = 4\pi \left[\frac{1}{2} x_{i+\frac{1}{2}}^2 + 2x_{i+\frac{1}{2}} x_{i-\frac{1}{2}} + x_{i-\frac{1}{2}}^2 \right] (x_{i+\frac{1}{2}} - x_{i-\frac{1}{2}}) \quad (7.14)$$

If \hat{V}_i was considered to be the volume between $x_{i+\frac{1}{2}}$ and $x_{i-\frac{1}{2}}$, then

$$\hat{V}_i = 4\pi \left[\frac{1}{3} (x_{i+\frac{1}{2}}^2 + x_{i+\frac{1}{2}} x_{i-\frac{1}{2}} + x_{i-\frac{1}{2}}^2) (x_{i+\frac{1}{2}} - x_{i-\frac{1}{2}}) \right] \quad (7.15)$$

It is not difficult to show that

$$\hat{V}_i - V_i = \frac{\pi}{3} (x_{i+\frac{1}{2}} - x_{i-\frac{1}{2}})^3. \quad (7.16)$$

A calculation done with \hat{V}_i in lieu of V_i is given in figure 19 and is labeled AVG_1 .

Another differencing scheme was suggested by L. A. Schmittroth, and it proceeds as follows from integrating the momentum equation by parts.

$$\rho \frac{\partial x}{\partial t} = - \frac{\partial p}{\partial x} \quad (7.17)$$

$$4\pi \int_{x_{1-l_2}}^{x_{1+l_2}} \rho \frac{\partial x}{\partial t} x^2 dx = -4\pi \int_{x_{1-l_2}}^{x_{1+l_2}} \frac{\partial p}{\partial x} x^2 dx \quad (7.18)$$

$$(\ddot{m}\ddot{x})_1 = -4\pi \left\{ (px^2) \left| \begin{matrix} x_{1+l_2} \\ x_{1-l_2} \end{matrix} \right. - 2 \int_{x_{1-l_2}}^{x_{1+l_2}} px dx \right\} \quad (7.19)$$

$$= -4\pi \left\{ (px^2) \left| \begin{matrix} x_{1+l_2} \\ x_{1-l_2} \end{matrix} \right. - \frac{p_{1+l_2} + p_{1-l_2}}{2} (x^2) \left| \begin{matrix} x_{1+l_2} \\ x_{1-l_2} \end{matrix} \right. \right\} \quad (7.20)$$

$$= -2\pi (x_{1-l_2}^2 + x_{1+l_2}^2) (p_{1-l_2} - p_{1+l_2}) \quad (7.21)$$

$$\ddot{x}_1 = 4\pi \frac{(x_{1-l_2}^2 + x_{1+l_2}^2)}{(m_{1-l_2} + m_{1+l_2})} (p_{1-l_2} - p_{1+l_2}) \quad (7.22)$$

In contrast to equation (7.10) which uses the area at the interface, equation (7.22) uses the average of the areas at the mid-point of the zones adjacent to the interface. The results of the calculation using difference equation (7.22) is given in figure 19 and is labeled AVG_2 . Similarly, if we let

$$\ddot{v}_1 = 4\pi \frac{x_{1+l_2}^2 + x_{1-l_2}^2}{2} (x_{1+l_2} - x_{1-l_2}), \quad (7.23)$$

then

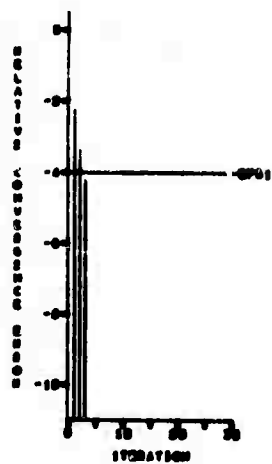
$$\ddot{v}_1 - v_1 = \pi (x_{1+l_2} - x_{1-l_2})^3, \quad (7.24)$$

HYRAD1 was then modified to calculate the zone centers and acceleration terms as given by equations (7.10) and (7.12) for the F^3 program. The results are also shown in figure 19.

7.3 Combined Radiation Diffusion and Hydrodynamics

The results of a combined radiation diffusion and hydrodynamic problem are shown here in figures 20 through 25. This problem is a multi-material calculation in which one material is heated and then transfers this energy to the other by radiation. The initial transfer of energy creates a shock in the second material as indicated by the formation of a spike in the pressure profile shown in figures 20, 21, and 22. This influx of energy causes the second material to expand one zone at a time back into the first material and also forward with the shock causing an increasing number of zones to be compressed at and immediately behind the leading edge of the shock wave. Note that from figure 23 on, the shock wave has overtaken and is accelerating ahead of the diffusion wave. This is indicated by the formation of the additional step within the temperature profile.

T 0.000000E+00
 DT 0.010000E-03 P
 NTA 000



ONEGATE1 .500
 ONEGATE2 .500
 ONEGATE3 .500
 ONEGATE4 .500
 TPAC .1000 DT 0.000E-00 10
 MPAC .0100 DM 1.000E-00 11
 CPAC .0000 DTC 0.000E-01 11
 MU 1.000 SIGMA 1.000
 IS 0.000E-00
 OS 0.000E-00
 SC 0.000E-00

CAL 1 ZONE MATERIAL -A THETA 0 -A P -1 -1 0.000E+00
 IS AL 1.000E-00 1.700E-01 0.010E+00
 TOTAL TIME .100
 CURRENT TIME .100

Figure 20

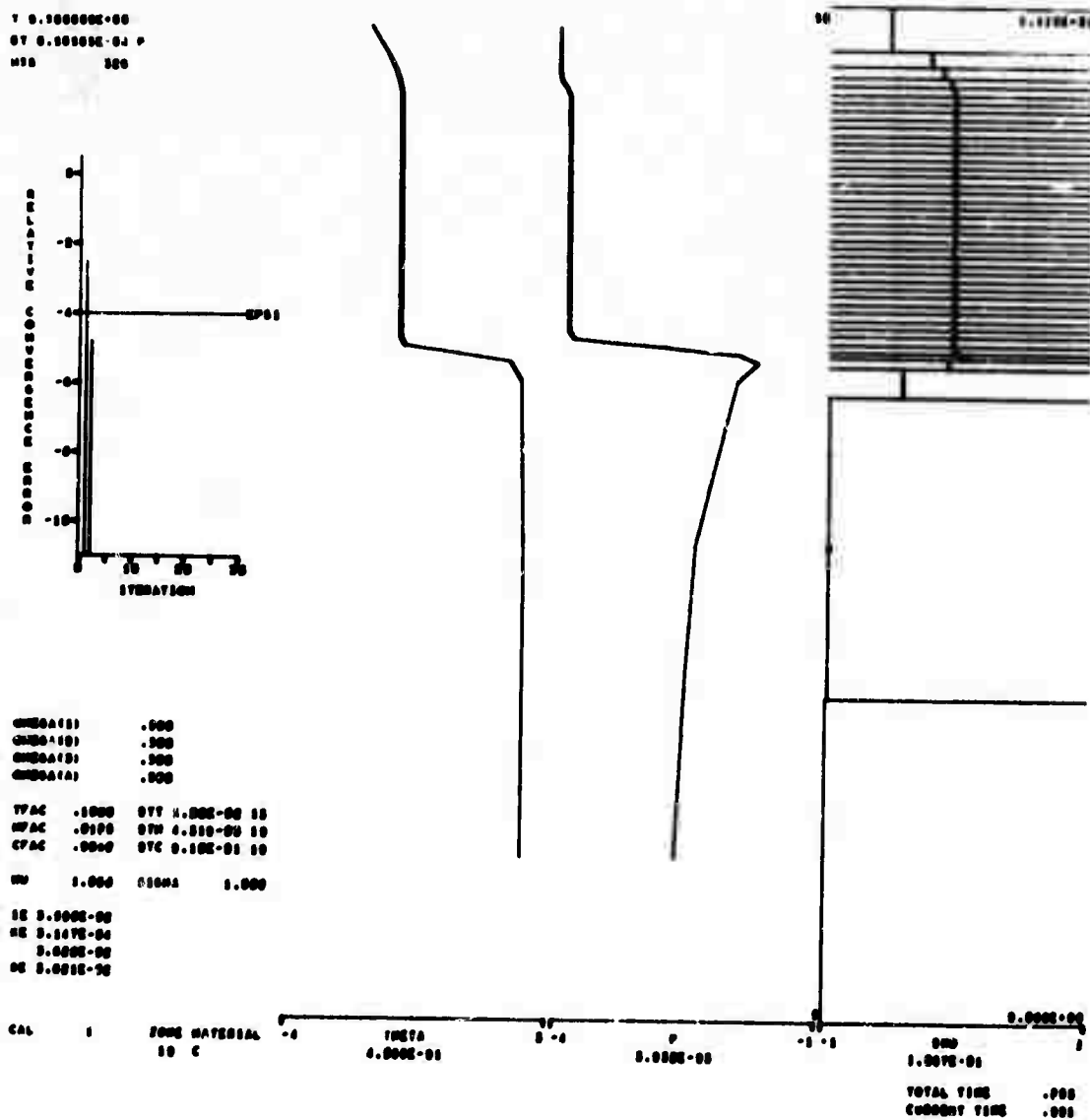
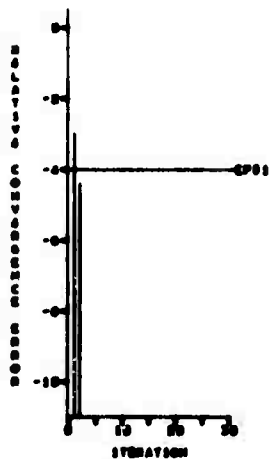


Figure 21

1 1.000000E+01
 DT 0.100000E-05 P
 NTS 440



CH20A(1) .000
 CH20A(2) .000
 CH20A(3) .000
 CH20A(4) .000
 TVAC .1000 DT 1.000E-05 10
 WTVAC .0100 DT 0.000E-05 10
 CVAC .0000 DT 1.000E-01 10
 CH 1.000 CH20A 1.000
 10 0.1075E-02
 10 7.070E-04
 0.070E-02
 0.070E-02

CAL 1 FORM MATERIAL -4 THETA 0.400E-03 0 -4 P 0.1000E-01 -1 -1 0.000E+00
 10 AL 0.000E+00
 TOTAL TIME .000
 COMPUT TIME .200

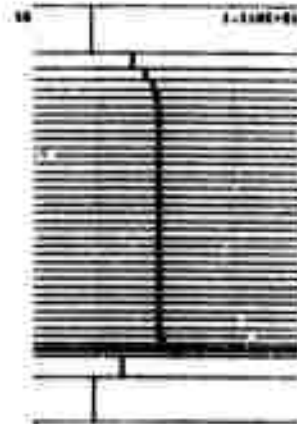
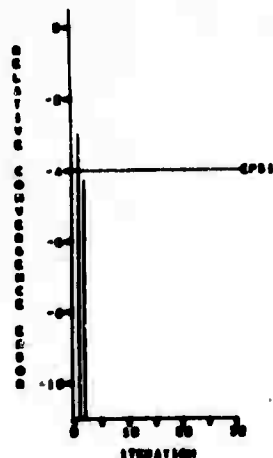


Figure 22

T 1.000000E+01
 DT 0.01010E+00 P
 NTS 100



CH00A(1) .000
 CH00A(2) .000
 CH00A(3) .000
 CH00A(4) .000
 CPAC .0000 DT 1.010E+00 20
 CPAC .0100 DT 0.000E+00 17
 CPAC .0000 DT 0.100E+00 10
 MU 1.000 21000 1.000
 10 0.010E+00
 20 1.000E+00
 40 0.000E+00
 60 0.000E+00

COL 1 2000 MATERIAL 0.000E+00 0.000E+00 0.000E+00 0.000E+00 0.000E+00
 10 PL 0.000E+00 0.000E+00 0.000E+00 0.000E+00 0.000E+00
 TOTAL TIME .010
 CURRENT TIME .010

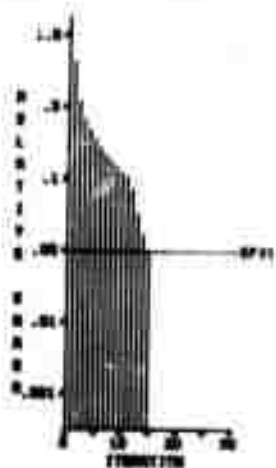
Figure 23

7.4 Summary

The selection of computer calculations included in this section is not exhaustive but rather illustrative. A great deal of work remains to be done, particularly within the areas of validating the non-linear approximation techniques, the hydrodynamic activity for various geometrical shapes and multi-material effects. Detailed studies also need to be made into the effects of the equation of state and opacity calculational schemes. For example, figure 26 illustrates a difficult yet convergent time step. Notice the plot of the relative convergence error at each iteration. The initial decay is a rather moderate exponential response which changes abruptly after the eleventh iteration.

The other plots on this figure show the change of several zone variables over the course of the time interval. The zone plotted is that which had the largest relative convergence error at iteration 15, the last iteration. The values plotted (from top left) are $\frac{\Delta c}{\Delta \theta}$, $\frac{\Delta \epsilon}{\Delta v}$, p , $\bar{\lambda}$, θ , the luminosity (flux times the area) into one end of the zone and out of the other, and a somewhat confusing and uninformative convergence graph which has since been dropped. The initial vertical line on the $\frac{\Delta c}{\Delta \theta}$ plot (labeled DEDT) is simply a line drawn from the base line to the value of $\frac{\Delta c}{\Delta \theta}$ as it was three time steps ago. The next two time step values are then plotted with a line between them giving a short curve which is representative of the behavior of the derivative over the previous three time steps. Another vertical line is then drawn from the base line up to the first iterative value of the term

T 1.242+00
DT 6.379-03 T
NTS 90



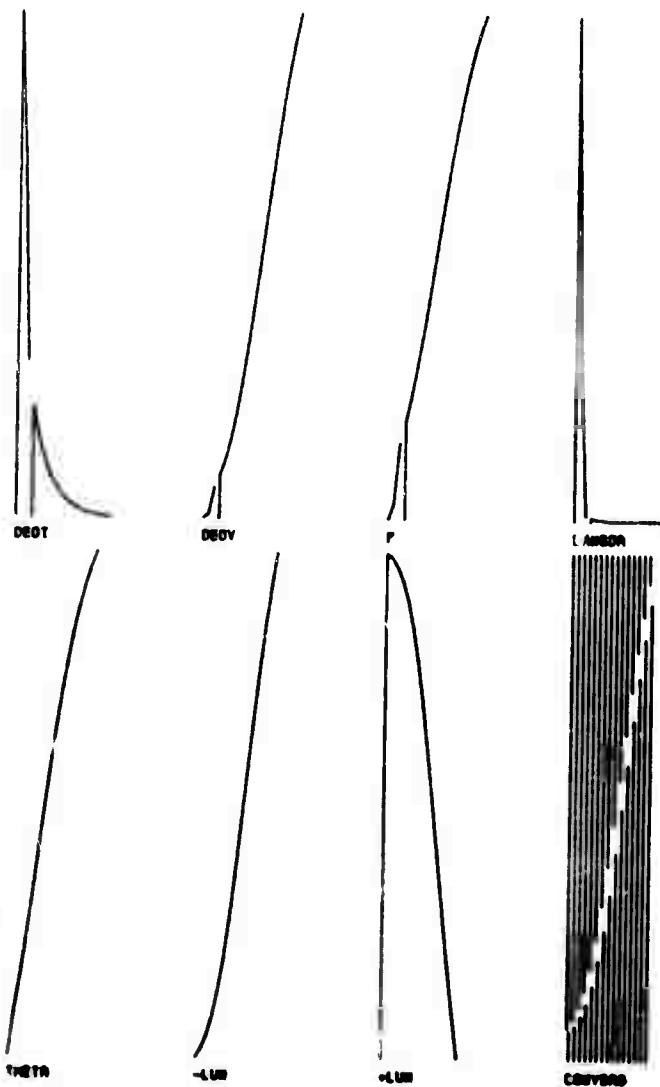
GO BACKUP WAIT
RECORD REZONE
SNAPSHOT DT/2
ABORT

NO 00000000
COUNT 4560+
7890000

TPRC -1000 REL.OTS 1.000-01
APRC -2000 REL.OTS 1000
OTS 1.000-00 CYMR 1.000-00
STP 10 MTS 100

SE 2.000-00 OTC 1.50-01 1
IS 2.027-00 OTH 1.50-01 1
NS 2.000-04 OTT 6.50-03 2
CTMR 3.5
OCTMR 3.5

3 RTH V



1.998-04

1.738-09

1.290-03

Figure 26

for the current time step and subsequent iterative values are represented by the curve following. This format is repeated for the $\frac{\Delta \epsilon}{\Delta v}$, p and $\bar{\lambda}$ terms (labeled DEDV, P and LAMBDA respectively). The curves for θ and the luminosity represent only the iterative values for the current time step and (unfortunately) do not include values for previous time steps.

Similarly, figure 27 is a picture of a time step which, while convergent, displays rather erratic behavior. Note that it initially starts to converge, abruptly diverges and then converges. Notice the corresponding graphs of the behavior of various zone quantities.

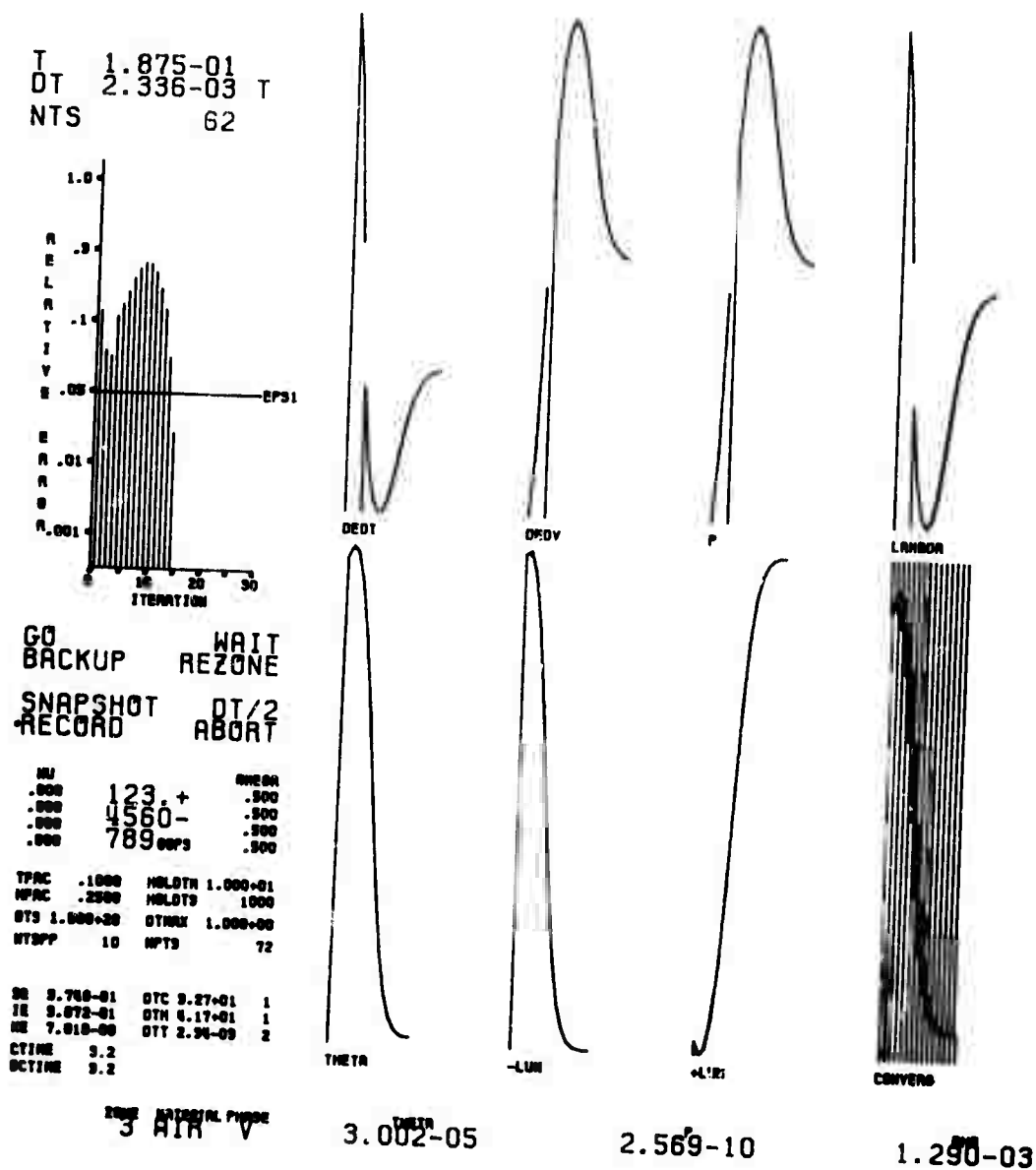
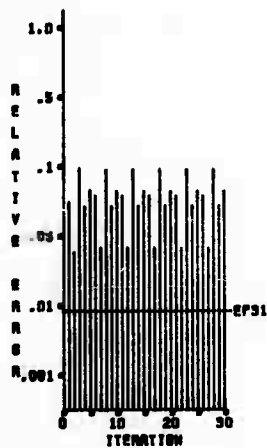


Figure 27

Figure 28 gives a snapshot of a time step which doesn't converge after thirty iterations. It also looks as if it will never converge and appears to oscillate every five iterations. Notice the insensitivity of the mean free path and one of the luminosity terms. The other luminosity term is somewhat affected, and the pressure even less affected by the fluctuations. Clearly, it is the behavior of the energy derivative terms which are causing the problem. A look into the equation of state tables for the material of this zone showed a discontinuity in these values near this temperature and density. As it turned out, a small increase in temperature resulted in a huge change in the derivatives due primarily to the linear interpolation scheme. Subsequently, the temperature dropped and again the corresponding derivatives changed drastically. Thus, the temperature (and corresponding quantities affected by it) oscillated back and forth about an entry in the equation of state tables, either side of which gave widely varying derivative values based upon linear interpolation. Decreasing ω_1 and ω_2 from 0.5 to 0.1 dampened out the oscillations and the calculations were able to proceed. Alternatives would be to raise the convergence limit, reduce the time step size, or any combination of these.

T 1.012-04
DT 1.663-05 T
NTS 19



GO WAIT
BACKUP REZONE
SNAPSHOT DT/2
RECORD ABORT

MU		OMEGA
.000	123. +	.500
.000	4560-	.500
.000	789 99F3	.500

TPAC	.1000	HOLDTH	1.000+01
HPAC	.2500	HOL' 3	1000
OTS	1.000+20	OTW	1.000+00
NTSPP	10	MPTS	29

SE	2.024-06	STC	7.11+03	1
TE	2.042-06	STH	7.28+03	2
RE	6.206-24	STT	1.00-05	1
CTIME	3.1			
DCTIME	3.1			

ZONE MATERIAL PHASE
I AIR V

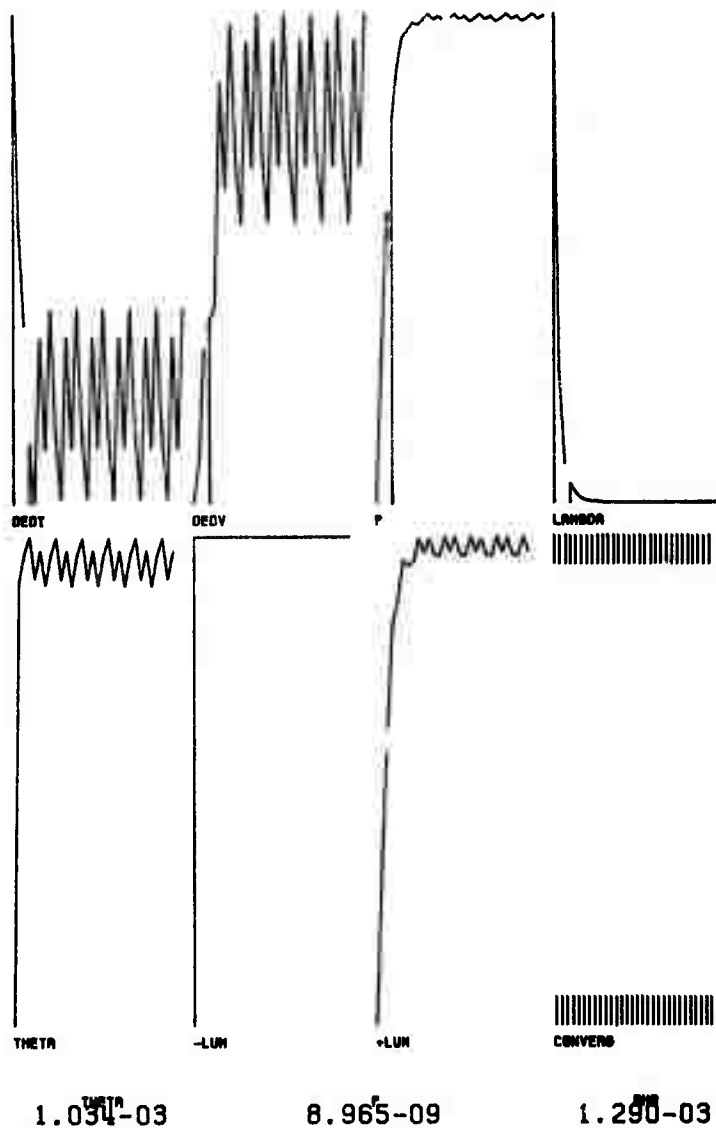


Figure 28

CONCLUSION AND AREAS FOR FUTURE RESEARCH

As stated in the introduction, the development of this system has extended over the past several years. During this period a variety of techniques have been tried within a number of different programmed solutions on four different computers. The end product consists of a highly polished machine language program which consumes huge amounts of time on the PDP-10 computer in contrast to the small amounts of time consumed by the relatively inefficient and unfinished FORTRAN version on the CDC-7600.

The PDP-10 version was originally coded in FORTRAN only to find out that the FORTRAN system on that computer was full of gross errors and inefficiencies. To obtain significant results on the PDP-10, the calculations for $\phi = 3^4$ and ΔV necessitated using double precision. After quickly determining that the DEC-supplied double precision routines were overly restrictive on the range of operands with which they could produce significant results (and contained minor errors), the method was reprogrammed in MACRO-10, the machine language for the PDP-10. As alluded to above, this also included a complete package of library routines for performing double precision arithmetic (addition, subtraction, multiplication, and division) in addition to some elementary mathematical functions (square root, natural log and exponential). To say the least, it is sad to think that a computer of this size has no double word arithmetic capability and that none of the modern computers have the hardware capability to perform the

elementary mathematical functions. It may be of interest at this point to mention that the double precision square root routine within the PDP-10 version of HYRAD1 consumes over 60% of the total calculational time.

In addition to the fact that the MACRO-10 version works and the FORTRAN version didn't, the resultant speed and storage improvement of the MACRO-10 version over the FORTRAN version on the PDP-10 was dramatic. The differences between the PDP-10, CDC-6600 and CDC-7600 are even more outstanding. A particularly simple problem which ran for 64 minutes on the PDP-10 in 29k words of core, used but 6 minutes on the CDC-6600 and a mere minute on the CDC-7600 in 32k words of core. Remember that this comparison is between a very efficient "hand crafted" program on the PDP-10 with a FORTRAN version on the CDC machines that is well known for its inefficient use of machine resources. It is worth noting that the same problem consumed .4 minutes using the non-iterative F^3 Los Alamos program and that HYRAD1 used an average of 6.1 iterations per time step, both taking nearly 2900 time steps. It is not unusual for a problem to run for several hours on the CDC-7600 computer.

It is clear that increased hardware functions are necessary for numerical calculations of this type. Not fast simple parallel functions as exhibited by the ILLIAC IV computer, but rather independently functioning units with increased capability (i.e. square root, exponential, etc.). Raw computing power is not enough though. A better man-machine interface needs to be developed. The user needs to retain control over the calculations rather than submitting to the crude demands of the machine.

As mentioned, this program was developed under a simple interactive (and sometimes graphical) system. The user was thereby able to alter parameters, introduce data changes, direct program control, and even make crude program patches. This was done to get, first of all, answers which may otherwise be very difficult to obtain under the traditional "batch" mode of processing. Secondly, through the interactive mode of operation, the user was able to get better answers in the sense that more resolution could be obtained at those times when it was required. Finally it was possible to get an immediate and in depth realization of the solution in moving picture form.

Slowly, but most certainly, tools are being created to provide such a man-machine interface. However, such tools have traditionally been improved interface equipment such as display consoles or they have been huge and rather obtrusive software systems which are programs to make up for the lack of sufficient and sophisticated hardware. Very large compilers are continually being developed at great expense to provide a more natural language interface between man and machine. However, all of them fall short on retaining enough information to relate back to the original language and to retain an overall view of what is being done. Thus, grand interpretive systems have been and are being developed which have some of these characteristics at great expense in both time and space.

Clearly the development of such software systems over the past several years is causing questions to be asked. Questions such as: Why not build machines to work at the user level? Why have compilers?

They generally discard most all of the useful information required as input anyway. Hardware is getting so fast and cheap, why not build computers that work in the infix mode directly (essentially) on the user's source program which can then be easily changed and debugged dynamically? Thus, why not build computers which add, multiply, etc. operands according to their definition at the point of execution be it integer, real, array, procedure or whatever?

There are so many situations which arise at run time that just can't be taken care of by the compiler, or the programmer ahead of time. This is true of problems in general despite the best planning. Therefore, why not defer the final decision making until such a time that it is in context? This technique is already in popular use for determining the final operand address. It seems to be a rather natural extension to go one step further and say that the add instruction, for example, is defined by the type and kind of operands upon which it is to operate. This then makes "add" a primitive which has no complete or definitive meaning by itself. Thus, the actual instruction set for a computer becomes very small and simple. There are no longer 2-5 different multiply instructions plus a host of multiply subroutines to handle things like the multiplication of arrays or complex numbers. There is just one multiply, and it is micro-programmed, i. e. you wish, by its operands.

In conclusion, the model developed herein and the subsequent calculations indicate that the numerical methods are reasonable and are capable of giving valid results. With the advent of better computing tools, the solution techniques appear even more palatable. The develop-

ment of the straight forward radiation diffusion scheme was an early (5 years ago) revolt against the first order expansion techniques as used by [5]. The results seem to bear out the fact that these equations are at least as good as those used in the past. Other recent analysis and work done, notably by Burton Wendroff [15], seem to indicate that this approach has a great deal of promise.

The iterative procedure was included for two purposes. First, it provides a corrective mechanism which tends to give better than first order resolution since it includes some foresight as well as hindsight. Secondly, it provides an easy way of incorporating non-linear effects. It is actually instructive to watch the iterative procedure sneak up to the answer via the display console. The anomalies are especially interesting as pointed out in section 7.4. Such iterative procedures have been successfully used for a long time in thermal and neutron diffusion programs.

Several other features of the model are also worth mentioning at this time. Probably next in order of importance is the opacity averaging scheme at the interface as given in section 5.2 even though its worth has not yet been fully determined. It appears to be the only scheme in use that has a sound mathematical and physical basis and yet still works [6]. This has been and continues to be a prime area for future work. Coming next in a close, yet, second place is the zone centering problem as exhibited by the point source and frustum calculations in section 7.3. The kinetic energy as approximated by (2.64) or the total energy conservation is incorrect for these problems. This discrepancy seems to be connected with the zone centering problem.

It is clear that more work needs to be done in this area [16]. Even the P^3 solution of the source problem is in suspect in light of the shock tube problem. It seems as though the calculational results should lag behind and achieve an asymptotic solution. Problems with the singularities at the center plus the fact that the source energy is actually introduced at the center of the first zone rather than actually at the center of the sphere tend to suggest a much harder look at the problem and the idealized solutions given in [12], [13] and [14].

Some of the other new and successful features include the Hydrodynamic Time Step Restriction procedure which guarantees that not only will zones not cross, but that they will not expand or compress too quickly. The implementation of the extensive equation of state and opacity table look-up procedures are not detailed herein, but are extensive, efficient and very fast. The technique of introducing energy into the problem by means of a temperature profile over several zones as given in section 6.2 is new in that it calculates the amount of energy required to bring the specified zones to that predetermined temperature. The iterative procedure plays a useful corrective role here too.

The one important feature not incorporated within the model is a dynamic reasoning procedure over which the user has final control, yet is automatic under certain user specified conditions. The P^3 program employs a procedure which will not initially calculate those exterior zones three or more zones away from the active zones. This technique helps to reduce the calculation time by not including those zones

which are not yet active (i.e. those zones which have not yet been affected by radiation or hydrodynamics). This scheme works only from the so called "inner boundary" (low zone numbers) outward and must have an "ambient" boundary condition at the other end. If the "outer" boundary condition is active, if there is a gradient near the "outer" boundary, or if there are non-zero source terms near the "outer" boundary, then the program must proceed to do the calculation for all zones regardless of what happens at the "inner" boundary or interior to the problem. It is desirable to generalize the technique with rezoning into more zones when needed, and likewise, recombining zones when no longer needed.

BIBLIOGRAPHY

1. Bird, R. B., Stewart, W. E., and Lightfoot, E. N., Transport Phenomena. John Wiley & Sons, Inc., New York, 1960, pp. 75, 76, 314.
2. Cox, A. N., "Stellar Absorption Coefficients and Opacities," Stars and Stellar Systems. Vol. 8, Edited by Aller, L. H. and McLaughlin, D. B., University of Chicago Press, Chicago, Illinois, 1965, pp. 198-201.
3. Richtmeyer, R. D. and Morton, K. W., Difference Methods for Initial-Value Problems. Interscience Publishers, Inc., New York, 1967.
4. Merts, A. L., and Stewart, J. N., Private Communications, Los Alamos Scientific Laboratories, Los Alamos, New Mexico, 1970.
5. Cox, A. N., Brownlee, R. R., and Eilers, D. D., "Time Dependent Method for Computation of Radiation Diffusion and Hydrodynamics," Astrophys. J. 144 (1966), 1024-1037.
6. Harlow, F. H. and Melixner, B. D., The Diffusion of Radiation. U.S. At. Energy Comm. Rept. LA-2196, 1958.
7. Eilers, D. D., Swihart, T. L., and Brownlee, R. R., Private Communications, Los Alamos Scientific Laboratories, Los Alamos, New Mexico, 1968.
8. Cox, A. N., and Stewart, J. N., "Radiative and Conductive Opacities for Eleven Astrophysical Mixtures," Astrophys. J. Suppl. Ser. 11, No 94 (1965) 22-46.
9. Petschek, A. G. and Williamson, R. E., The Penetration of Radiation With Constant Driving Temperature. U.S. At. Energy Comm. Rept. LAMS-2421, 1960.
10. Crowley, S. K., A Comparison of Analytical and Numerical Solutions for the Shock Tube Problem. U.S. At. Energy Comm. Rept. UCRL-14198, 1955.
11. Harlow, F. H., and Amsden, A. A., Fluid Dynamics: An Introductory Text, U.S. At. Energy Comm. Rept. LA-4150, 1970.
12. Thomas, J. D., Present Status of the Problem of Computing the Propagation of a Strong Shock Wave in Air, Los Alamos Sci. Lab. Memo J-10-292, 1957.

13. von Neumann J., and Richtmeyer, R. D., "Method for the Numerical Calculation of Hydrodynamic Shocks," J. Appl. Phys. 21 (1950), 232.
14. Brode, H. L., "Numerical Solutions of Spherical Blast Waves," J. Appl. Phys. 26 (1955).
15. Wendroff, B., The Initial Value Problem, University of Denver Rept. MS-6904, 1967.
16. Crowley, B. K., "PUFL, An Almost-Lagrangian Gasdynamic Calculation for Pipe Flows with Mass Entrainment," J. Comp. Phys. 2 (1967), 61-86.